2005

Studies Of Liquid Crystal Response Time

Haiying Wang
University of Central Florida

STUDIES OF LIQUID CRYSTAL RESPONSE TIME

by

HAIYING WANG
B.S. Hangzhou Dianzi University, P.R. China, 1992
M.S. Hangzhou Dianzi University, P.R. China, 1995
M.S. University of Central Florida, 2004

A dissertation submitted in partial fulfillment of the requirements
for the degree of Doctor of Philosophy
in the Department of Electrical and Computer Engineering
in the College of Engineering and Computer Science
at the University of Central Florida
Orlando, Florida

Fall Term
2005

Major Professors: Shin-Tson Wu
Thomas X. Wu

ABSTRACT

In this dissertation, the response time issue of the liquid crystal (LC) devices is investigated in meeting the challenges for display and photonic applications. The correlation between the LC director response time and the optical response time is derived theoretically and confirmed experimentally.

This thesis begins with a description of liquid crystal materials and their physical properties, and then introduces the simulation methodologies. These brief but relevant introductory chapters pave the foundation for fully understanding the dynamic response of LC devices. After that, three chapters pertaining to optical response time are presented.

A major contribution of this thesis is that, based on the small angle approximation, we derive rigorous analytical solutions for correlating the LC director response time to its consequent optical response times (both rise and decay) of a vertical-aligned nematic LC cell. Pretilt angle effect on the LC dynamics is studied, and it is found that a modified rotational viscosity is needed in order to explain the experimental results. Grayscale switching is also analyzed numerically. This work successfully fills the gap in the literature of LCD switching dynamics.

An important effect related to response time, backflow is analyzed using a homogeneous LC cell in an infrared wavelength. Due to the relatively high voltage applied in an optical phased array (OPA), the backflow effect which takes place in the first few milliseconds influences the LC response time dramatically. However, the corresponding Leslie viscosity coefficients, which are crucial in investigating the dynamic response of LC devices with backflow, can hardly be found in the literature. A new effective approach to estimate the Leslie coefficients of LC

mixtures based on MBBA data is proposed in this dissertation. Using this method, the Leslie coefficients of the LC material under study can be extracted based on its order parameters. The simulation results agree with the experimental data very well. This method provides a useful tool for analyzing the dynamic response including backflow, in order to obtain accurate optical response time under a high biased voltage.

Cell gap is an important factor affecting the LC response time. Usually a thinner cell gap is chosen to achieve faster response time, since normally both rise and decay times are known to be proportional to d^2. However, they are valid only in the $V_{th} < V < \sqrt{2}V_{th}$ region, where V_{th} stands for the threshold voltage of an LC cell. In the large voltage region where $V_{\pi} < V < V_i$, the optical decay time is *independent* of *d*. In this thesis, we find that between these two extremes the response time is basically *linearly* proportional to *d*. Our analytical derivation is validated by experimental results. Therefore, in the whole voltage region, the physical picture of the optical response time as a function of the cell gap is completed. This analysis is useful for understanding the grayscale switching behaviors of the LC phase modulators. With the help of cell gap effect in phase modulator, we can effectively reduce the response time by using a thick cell or double cells to achieve the intended phase retardation in an anticipated operating wavelength.

In conclusion, this dissertation has solved some important issues related to LC optical response time and supplied valuable tools for scientists and engineers to numerically analyze the LC dynamics.

To Yunjing and Liping

ACKNOWLEDGMENTS

I would like to thank those who contributed and supported my efforts throughout my graduate studies at the University of Central Florida. First and foremost I wish to record my gratitude to my advisor, Dr. Shin-Tson Wu for his financial support during these years, without that, I couldn't have continued my graduate studies at UCF. Meantime, I would like to thank him for his creative sense，constant help, motivation and valuable guidance in this area, which opens a new wider world to me—Liquid Crystal. I would like to thank him for his detailed and kind instructions in the laboratory, for his patience and instruction to improve my oral and written English skills.

I am sincerely indebted to my advisor, Dr. Thomas X. Wu for his enlightening discussion on derivation of the correlation function about the optical and director response times. I would like to thank him for his patience and time to polish my manuscripts. Under his guidance, I have gotten deeper knowledge in electromagnetic field. I have also improved my capability to perform numerical simulation, which includes Finite Element, Finite Difference, and other methods.

I would also like to thank my dissertation committee members, Dr. Aniket Bhattacharya, Dr. Issa Batarseh, and Dr. Juin J. Liou, for their help and invaluable suggestions in my dissertation.

I gratefully acknowledge all the Postdoctoral Fellows in the Photonics and Display group and in particular Dr. Xinyu Zhu and Dr. Yuhua Huang for their helpful discussions in liquid crystal displays. I appreciate Dr. Yanqing Lu for his intensive preparation and positive attitude. I am indebted to Dr. Hongwen Ren and Dr. Sebastian Gauza for mentoring me in the experiments. I would like to give thanks to Dr. W. K. Choi for his mentorship in 2-D dimMOS and Simulation

software as well as useful discussion in technical issues.

I am grateful to all the students in the Photonics and Display group and High-Speed Electronic System groups, most of them have helped me in one way or another. In particular I would like to thank Dr. Claire Y. Fan, Ms. Yi-Hsin Lin, and Ms. Chien-Hui Wen, for their help and encouragement.

Finally, it is a pleasure to give thanks to my husband, Liping Zheng. He also pursued his Ph. D. degree this period and we have a lovely young daughter to be taken care of by ourselves. He lives cheerfully and without complaints. I am forever grateful to my parents for their moral support during this period.

TABLE OF CONTENTS

LIST OF FIGURES

LIST OF TABLES

LIST OF ACRONYMS/ABBREVIATIONS

AM	Active-Matrix
CRT	Cathode Ray Tube
DAP	Deformation of Aligned Phases
DCC	Dynamic Capacitance Compensation
FLC	Ferroelectric Liquid Crystal
FoM	Figure of Merit
IO theory	Imura and Okano Theory
IC	Integrated Circuits
LC	Liquid Crystal
LCD	Liquid Crystal Display
MTN	Mixed-mode Twisted Nematic
MCIF	Motion-Compensated Inverse Filtering
MVA	Multi-domain Vertical Alignment
OPA	Optical Phased Arrays
OCB	Optical Compensation Bend
PDLC	Polymer Dispersed Liquid Crystal
PNLC	Polymer Network Liquid Crystal
SLM	Spatial Light Modulator
TFT	Thin Film Transistor
VA	Vertical-Aligned

CHAPTER 1: INTRODUCTION

1.1 Motivation

Liquid crystal technology, which is related to multi-disciplinary science, has found its way into every modern household in displays and photonics. In display area, liquid crystal displays (LCDs) can be found in handheld (0.5-4″), notebook computers (10-15″), desktop monitors (15-21″), LCD-TVs (17-46″+), HDTVs (82″), and digital movies (42'×27'). In mobile communications, LCDs are commonplace in palm pilots, handheld terminals, mobile Internets, wearable computers, wearable TVs, and car navigations. In photonics area, liquid crystal (LC) spatial light modulator (SLM) has been used as a phase-only modulation for laser beam steering, tunable-focus lens, and other photonic devices. Liquid crystal devices have been improved remarkably over the last several years. Moreover, innovation has been taking place every one and a half years.

LCDs have unique features such as flat and compact structure, high image quality, low cost, low power consumption than Cathode Ray Tubes (CRTs), and they are easily interfaced with integrated circuits (IC). However, there are still some technical issues remain to be overcome. Compared to flat screen CRTs and Plasma monitors, their video refresh rate is slower, and the viewing angles are narrower. In this dissertation, we focus on the response time issue.

For TV applications, LCD is expected to displace CRT very soon, as it does in the computer monitors. The rapidly shifting videos require the LC device to operate at the true video rate that is less than 16 ms. However, the response time of LCDs using nematic is still not fast

enough for video display. Blurred edges in moving images impede its acceptance in the TV market.

For transmissive LCDs, the present response time (rise + decay) is approaching 10 ms, but in some fast-moving pictures, the response time should be less than 5 ms. For projection displays, the response time could be faster than 16 ms, thanks to the thermal effect of the high power lamp. In handheld displays, the response time in the Guest-Host (GH) display is about 50 ms and that in the Mixed-mode Twisted Nematic (MTN) mode is ~20 ms, depending on the cell gap. However, for a color sequential microdisplay, the required frame time should be less than 1 ms. This presents a technical challenge to nematic LCDs, especially in the low temperature region.

In meeting the challenges, the goal of this research work is to discover the appropriate fast response approaches of LC devices. In pursuit of improving the response time of nematic LCDs, a lot of approaches have been carried out. For instance, to improve the material performance new molecular structures with low rotational viscosity (γ_1) and high birefringence (Δn) [1],[2] have been developed. With the adaptive overdrive and undershoot method conceived in late 1980s [3],[4], the intrinsic slow inter-gray response time can be reduced to less than one fourth that of the conventional method [5],[6]. With the introduction of Dynamic Capacitance Compensation (DCC) for active-matrix (AM) LCDs in 2000 [7], LCDs made a jump in image quality. By incorporating DCC driving scheme and faster liquid crystal material, Samsung developed a TFT-LCD with all gray levels less than 10 ms [8].

Among all LC modes, Optically Compensated Bend (OCB) mode has the fastest response potential. However, two major technological issues still need to be addressed: 1) how to speed up the initial 'splay to bend' transition, and 2) how possibly to accomplish an excellent image quality

that surpasses those of conventional wide viewing LCD modes. To realize its bend transition at a low voltage and speed up this transition, Uchida group [9] studied bend-shaped polymer network formation and Bos group [10] developed high pretilt alignment layer to keep the bend orientation at low voltage. Nakamura et al. [11] proposed a method to speed up the 'splay to bend' transition by applying repeated pulse type bias voltage. Ezhov et al. [12] developed a 3D system based on LC-shutters and polarization switchable large panels. Lee group [13] developed new driving method in 17.0" SVGA panel to speed up the initial splay to bend transition time and without sacrificing the performance of OCB panel.

To achieve fast response time, several approaches have been reported. One approach is to use dual-frequency liquid crystal (DFLC) materials [14],[15]. In a DFLC device, electric field is present during both turn-on and turn-off periods to accelerate the LC reorientation processes. As a result, the rise and decay times are greatly improved. However, a DFLC material is a mixture containing positive and negative $\Delta\varepsilon$ LC components. Therefore, their $\Delta\varepsilon$ values at low and high frequency regimes are not large. That means, the required operating voltage is relatively high. Moreover, the crossover frequency shifts noticeably as the operating temperature increases. This makes precise grayscale control difficult.

Polymer network liquid crystal (PNLC) [16] exhibits a fast response time. Usually, a PNLC scatters light in the visible region. However, as the wavelength increases, light scattering diminishes in the λ=1.55 μm region. For a 12-μm planar LC cell, the response time for achieving a 2π phase change is about 2 ms at room temperature. However, due to the 10 wt% polymer concentration and small network domains, the operating voltage is relatively high, 7 V_{rms}/μm. To reduce voltage, a high birefringence and large $\Delta\varepsilon$ LC material needs to be developed.

Liquid crystal response time is limited by its slow free relaxation. To shorten its decay time, another orthogonal electrode along the substrate is suggested, which is used to control its decay process. In other words, the decay is driven by the electric field. The concept of this crossed-field effect was first proposed in 1975 [17], however, it had not been actually implemented in display devices because of the following shortcomings: high voltage, low contrast, more complicated driving, more complicated structure, and non-uniform transmission. In the past two years, Xiang et al. [18]-[22] analytically explored the electro-optic properties of VA and HAN cells with different electrode configurations (three electrodes [18]-[20] or four electrodes [21],[22]) to achieve a fast decay time using the crossed-field effect.

To improve on the motion image quality, Lee et al. [7] and Pan et al. [23] independently found that the slow response of LCD is not a dominant factor of motion blur. The slow response of LCD only contributes to 30% of the motion blur, while the hold-type rendering mode contributes to 70%. To reduce the hold-type motion blur, several companies, such as Samsung, Philips, NEC, et al. have some useful solutions. The first approach is to introduce an impulsive behavior to the transmittance, either by inserting black data between every two frames [24], or by using blinking backlight to eliminate the flickers [25],[26]. However, these solutions have the intrinsic shortcomings of low transmittance and contrast ratio. Another approach is to double the frame rate [27]. However, it requires extensive signal processing especially for motion estimation and interpolation. Phillips applied MCIF (Motion-compensated inverse filtering) on a 30” LCD-TV pane in 2004 and obtained a CRT-like display without motion blurring [28].

1.2 Thesis Overview

The research work discussed in this dissertation covers liquid crystal devices with a goal of meeting the response time challenges for displays and optical communications. It can be divided into three categories: 1) Motivation and introduction, 2) Various novel electro-optical effects that related to optical response time in nematic LC mixtures, and 3) Summary.

The dissertation is organized as follows.

Chapter 2 introduces the LC mixtures and their corresponding physical properties.

Chapter 3 reviews the numerical simulation methods for liquid crystal devices.

In Chapter 4, we give the detailed derivation of the correlations between the LC director reorientation time and the optical response (both decay and rise) time of a Vertically Aligned (VA) cell. Pretilt angle effect in response time is also calibrated by the modified rotational viscosity.

In Chapter 5, an important effect related to response time, backflow is analyzed using a homogeneous LC cell at λ =1.55 μm, which is commonly used for laser communication. Due to the relatively high voltage applied in an optical phased array, the backflow takes place in the first few milliseconds. We have modified the expressions of two Leslie coefficients (α_1 and α_2) in order to extend their validity to two high birefringence LC mixtures, E7 and UCF-2 based on the Imura and Okano (IO) theory. With these modifications, the simulation results agree quite well with the experimental data.

In Chapter 6, an interesting approach to achieve fast response time was investigated. This chapter provides a complete physical picture of optical response time as a function of cell gap (d) in a wide voltage regime. Normally both rise and decay times are known to be proportional to d^2

in the small angle approximation ($V_{th} < V < \sqrt{2}V_{th}$), and in the high voltage regime where $V_{\pi} < V < V_i$ the optical decay time is *independent* of *d*. In this chapter, we found that between these two extremes, there is a region where the response time is *linearly* proportional to *d*. Our analytical derivation is confirmed by experimental results.

Finally, in Chapter 7, we summarize the key achievements for this dissertation.

CHAPTER 2: LIQUID CRYSTAL MATERIALS AND PHYSICAL PROPERTIES

Although liquid crystal only occupies a small portion in an LC device, it plays a key role in determining the device performances. For example, the LC material and molecular alignment jointly determine the device contrast ratio, operation voltage, response time, viewing angle, and operating temperature. Even the material stability is critical to the lifetime of the devices. LC material is the fundamental of the whole LCD industries and researches. Therefore, this chapter will briefly introduce the LC classes and its important physical properties.

2.1 LC Mixtures

Liquid crystal is an organic molecule. Liquid crystals possess physical properties that are intermediate between solid crystals and isotropic liquids [29]. They have the flow and conformability properties of liquid, but exhibit crystalline properties, e.g., optical, dielectric, and elastic anisotropies, when the LC molecules are aligned by a surfactant. There are three major LCs of interest: thermotropic, lyotropic, and polymeric. Among these three, the thermotropic LCs have been studied extensively and their applications mature. Thermotropic LCs can exist in three phases: nematic, smectic and cholesteric, as illustrated in Figure 1.

In the nematic phase shown in Figure 1(a), the rod-like molecules are, on average, line up parallel to a preferred direction, which is characterized by a unit vector **n**, called the director. The director can be reoriented by an external electric field when the applied voltage exceeds the Freedericksz transition threshold. Since the liquid crystals are birefringence media, the field-induced director reorientation imparts a large phase changes on a traversing wave. Due to their

simple molecular alignment and natural gray scale capability, nematic LCs have become the mainstream for display and tunable photonics applications. In our research interest, emphasis is mainly on the nematic phase.

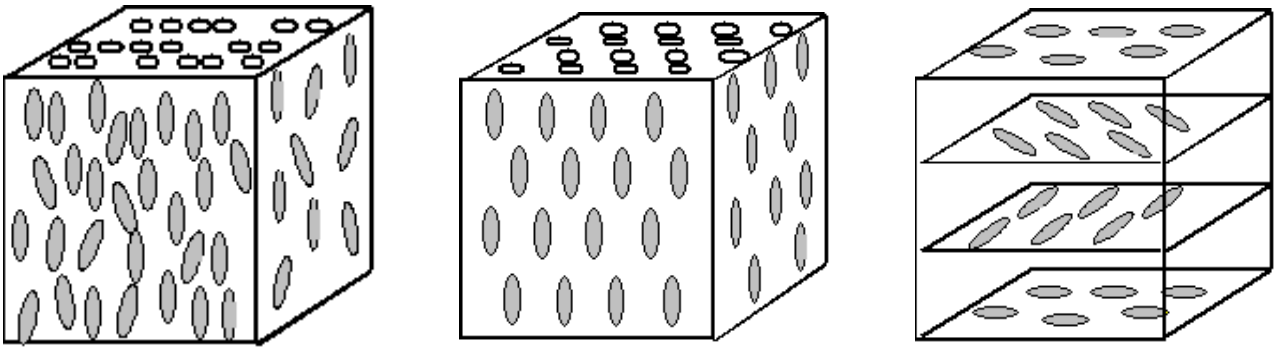

(a) (b) (c)

Figure 1: Schematics of three thermotropic LCs: (a) nematic, (b) smectic, and (c) cholesteric.

In the smectic phase shown in Figure 1(b), the molecules are in layered structures and arrange well with each other. There are at least nine distinct phases depending on the degree of ordering within those planes. An exciting feature of the chiral smectic-C phase is that it exhibits ferroelectricity. Using its spontaneous polarization, the response time of a bistable ferroelectric liquid crystal (FLC) modulator is in the 10-100 μs range. FLC has been demonstrated on a silicon backplane for virtual and projection displays [30]. Due to its fast response time, the FLC can perform color sequential and pulse-width modulation to obtain gray scales. In the cholesteric phase shown in Figure 1(c), it is thermodynamically equivalent to nematic phase except for the chiral-induced helix in the directors. There is parallel ordering in the same plane, but helical rotation along the axis perpendicular to different planes. The LC directors follow the helical

rotation of the chiral. The polarization states of the reflected and transmitted waves depend on the pitch length of the cholesteric. Because of its bistable nature (low power consumption), the cholesteric display is an attractive candidate for electronic books [31].

2.2 Basic Physical Properties

Liquid crystal exhibits a certain degree of order in the molecular arrangement. As a result, there is anisotropy in the mechanical, electrical, magnetic, and optical properties. A number of unique characteristics make LC particularly suitable for displays. For electro-optic applications employing a nematic LC, birefringence, elastic constants, dielectric anisotropy, and rotational viscosity all play important role affecting the device performance. The following sections will give an overview on the basic physical properties of LC materials.

2.2.1 Birefringence

The birefringence ($\Delta n = n_e - n_o$) of a uniaxial liquid crystal represents the difference between the refractive indices of the extraordinary ray (n_e) and the ordinary ray (n_o). High birefringence LC materials are essential for both display and optical communication applications [32]. For a cholesteric liquid crystal display (Ch-LCD) [14],[31], the reflection bandwidth ($\Delta\lambda$) is linearly proportional to the LC birefringence and pitch length (p) as: $\Delta\lambda = \Delta n \cdot p$. In the visible spectral region, the pitch length is ~350 nm. Thus, if Δn =0.6, then $\Delta\lambda$ =210 nm which would resemble a normally white Ch-LCD. For a Polymer-Dispersed Liquid Crystals (PDLC) [33],[34] or holographic PDLC [35], high Δn enhances the light scattering efficiency and thus improves the display contrast ratio. For fiber-optic switches (λ =1.55 μm) using optical phased arrays [36],

the required phase change ($\delta = 2\pi d\Delta n/\lambda$) is 2π. If we want to retain the cell gap d =4 μm to achieve a fast response time, the required Δn should be ~0.4 at λ =1.55 μm, which implies Δn ~0.5 in the visible region.

In order to describe the refractive index dispersion of LC materials, two issues need to be taken into account: wavelength effect and temperature effect.

2.2.1.1 Wavelength Effect

Vuks proposed the following equation to correlate the macroscopic observables (refractive indices) of an anisotropic LC to its microscopic properties (the molecular polarizability α) [37]:

$$\frac{{n_{e,o}}^2 - 1}{\langle n^2 \rangle + 2} = \frac{4\pi N}{3}\alpha_{e,o}, \tag{2.1}$$

where $\langle n^2 \rangle = (n_e^2 + 2n_o^2)/3$ is the average value of the refractive indices in the nematic phase, N is the number of molecules per unit volume.

Wu proposed a single-band model, where the wavelength-dependent birefringence of a LC can be expressed as follows [32],[38],[39]:

$$n_e(\lambda, T) \approx n_i(\lambda) + \frac{2}{3}GS\frac{\lambda^2\lambda^{*2}}{\lambda^2 - \lambda^{*2}}, \tag{2.2}$$

$$n_0(\lambda, T) \approx n_i(\lambda) - \frac{GS}{3}\frac{\lambda^2\lambda^{*2}}{\lambda^2 - \lambda^{*2}}, \tag{2.3}$$

$$\Delta n = G\frac{\lambda^2\lambda^{*2}}{\lambda^2 - \lambda^{*2}}. \tag{2.4}$$

In Eq. (2.4), the parameter $G = gNZS(f_{//}^{*} - f_{\perp}^{*})$ is temperature dependent but wavelength independent, and λ^{*} is the mean electronic transition wavelength. For a LC substance, the electronic transition bands are located in the UV region.

Equation (2.4) involves two parameters G and λ^{*}. Thus, by measuring the birefringence at two wavelengths, these two parameters can be determined and the entire birefringence dispersion curve can be obtained. From Eq. (2.4), as the wavelength increases, Δn decreases gradually and saturates in the near infrared region. In the IR or millimeter region where $\lambda >> \lambda^{*}$, Eq. (2.4) is reduced to $\Delta n \approx G\lambda^{*2}$, except in the vicinities of some local molecular vibration bands.

In the IR region, some harmonics of molecular vibration bands exist. Figure 2 and Figure 3 show the wavelength-dependent birefringence curves of two eutectic mixtures E-7 (cyano-bipheny mixtures) and ZLI-1132 (cyano-phenyl-cyclohexanes mixtures) in the visible and IR region, respectively, at room temperature. The dashed lines represent the theoretical results using Eq. (2.4). In Figure 3, positive dispersion of C≡N bonds (centered at 4.5 μm) and C-H bands (~3.4 μm) are observed in both materials. As a result, the intrinsic absorption can be relatively large depending on the detailed molecular composition. An LC with a long alkyl chain would enhance the absorption intensity of the C-H band. The birefringence saturates in the near infrared region except in the vicinities of some local molecular vibration bands. The measured birefringence results (E-7 and BL006 at 30GHz are 0.192 and 0.223, respectively) by Lim [40] are consistent with this analysis.

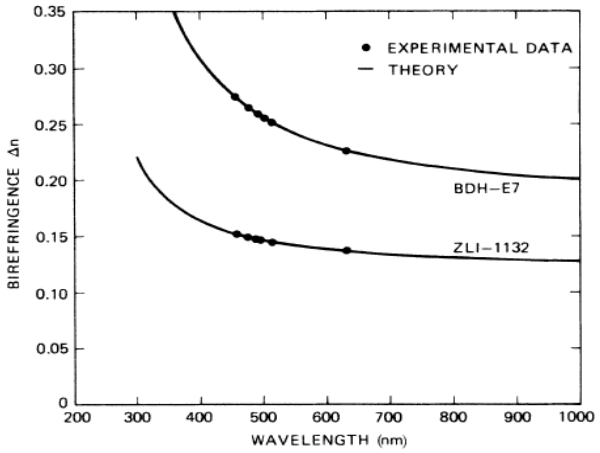

Figure 2: Wavelength-dependent birefringence in VIS [38].

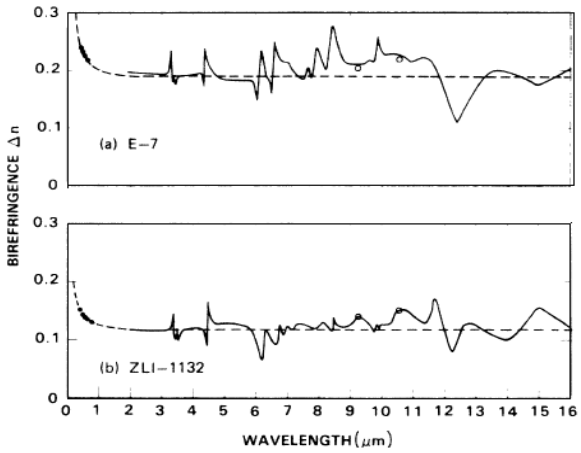

Figure 3: Wavelength dependent birefringence in IR [38].

Wu also proposed a three-band model, which takes all three electronic transition bands: one $\sigma \to \sigma^*$ and two major $\pi \to \pi^*$ into consideration [41],[42]:

$$n_e(\lambda) = 1 + g_0^e \frac{\lambda^2 {\lambda_1}^2}{\lambda^2 - {\lambda_o}^2} + g_1^e \frac{\lambda^2 {\lambda_1}^2}{\lambda^2 - {\lambda_1}^2} + g_2^e \frac{\lambda^2 {\lambda_2}^2}{\lambda^2 - {\lambda_2}^2}, \tag{2.5}$$

$$n_0(\lambda) = 1 + g_0^o \frac{\lambda^2 {\lambda_1}^2}{\lambda^2 - {\lambda_1}^2} + g_1^o \frac{\lambda^2 {\lambda_1}^2}{\lambda^2 - {\lambda_1}^2} + g_2^o \frac{\lambda^2 {\lambda_2}^2}{\lambda^2 - {\lambda_2}^2}, \tag{2.6}$$

where $g_i \sim NZ_i f_i$ are proportionality constants, Z_0 is the number of σ electrons, and $Z_1 = Z_2$ is the number of π electron in the LC mixture. In the off-resonance region, the three-band model ($\Delta n(\lambda \to \infty) \approx 0.16$) agrees well with measured birefringence results (5CB at 35 GHz are 0.158). For LC molecules with mainly saturated bonds (such as CH_3, CH_2, C_6H_{12}), the $\sigma \to \sigma^*$ transitions makes the primary contribution to birefringence. Their resonance wavelength is in deep UV (<180 nm) so that their birefringence is low. While for the LC molecules with unsaturated bonds (such as phenyl ring), the two $\pi \to \pi^*$ transitions make dominant contribution to LC birefringence. As conjugation length increases, $\pi \to \pi^*$ transition is more important. The first $\pi \to \pi^*$ transition band (λ_1) stays at around 210 nm while the second $\pi \to \pi^*$ transition band (λ_2) increases rapidly toward the visible wavelength [41] resulting in a higher birefringence.

Wu et al. [42] and Li et al. [43] extended the Cauchy equations to LC mixtures:

$$n_e = A_e + \frac{B_e}{\lambda^2} + \frac{C_e}{\lambda^4}, \tag{2.7}$$

$$n_0 = A_o + \frac{B_o}{\lambda^2} + \frac{C_o}{\lambda^4}, \tag{2.8}$$

where $A_{e,o}$, $B_{e,o}$, and $C_{e,o}$ are the Cauchy coefficients of the LC. This model fit the experimental data well in the off-resonance spectral region.

2.2.1.2 Temperature Effect

Temperature is another important factor affecting LC refractive indices. The temperature-

dependent refractive index is governed by the order parameter S in Eqs.(2.2) and (2.3), where S is described as:

$$S = (1 - T / T_c)^{\beta} \tag{2.9}$$

Eq. (2.9) is Haller's approximation for the order parameter. This approximation holds reasonably well if the temperature is not too close to the clearing temperature (T_c). The exponent β is dependent on molecular structure, not on wavelength. For most LC compounds studied, β is around 0.20-0.25.

Li et al. derived the four-parameter model for describing the temperature effect on the LC refractive indices [44]:

$$n_e(T) \approx A - BT + \frac{2(\Delta n)_0}{3}(1 - \frac{T}{T_c})^{\beta}, \tag{2.10}$$

$$n_0(T) \approx A - BT - \frac{(\Delta n)_0}{3}(1 - \frac{T}{T_c})^{\beta}. \tag{2.11}$$

Figure 4 plots the measured temperature-dependent refractive indices of 5CB (K 24 N 35.3 I) at three wavelengths: λ =450, 550, and 650 nm, respectively. The filled data points are for n_o, while the open points are for n_e. The solid lines are fitting results using the four-parameter model. The agreement is excellent. As the temperature increases, the refractive index decrease gradually, this trend is more pronounced as temperature approaches T_c. For a high T_c mixture, its refractive index is less sensitive to temperature in the vicinity of room temperature.

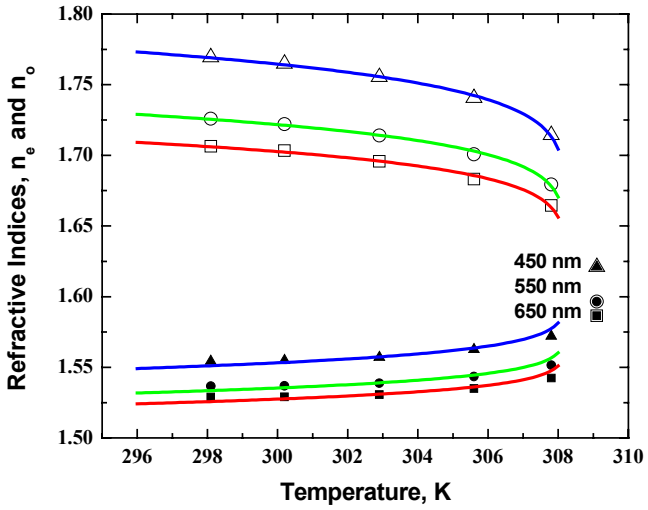

Figure 4: Temperature-dependent refractive indices of 5CB at $\lambda = 450$ (triangles), 550 (circles) and 650 nm (squares). Open dots are for n_e and closed dots are for n_o [43].

By taking temperature derivation of Eqs. (2.10) and (2.11), Li et al. further derived the following equations [44]:

$$\frac{dn_e}{dT} = -B - \frac{2\beta(\Delta n)_0}{3T_c(1-\frac{T}{T_c})^{1-\beta}}, \tag{2.12}$$

$$\frac{dn_0}{dT} = -B + \frac{\beta(\Delta n)_0}{3T_c(1-\frac{T}{T_c})^{1-\beta}}. \tag{2.13}$$

This implies that n_e decreases as the temperature increases throughout the entire nematic range, while n_0 may initially increase or decrease with temperature, depending on the sign of Eq. (2.13). As T approaches T_c, dn_0/dT jumps to a large positive number. In the intermediate, there exists a transition temperature (T_0) where dn_0/dT =0. Li et al. analyzed two critical parameters

affecting dn_0 / dT , which are high birefringence and low clearing temperature. Based on this, they formulated two exemplary LC mixtures using the laterally substituted isothiocyannato compounds.

The birefringence effect on the response time is through the cell gap dependence. High birefringence LC materials lead to a thinner cell gap which, in turn, reduces the response time.

2.2.2 Dielectric Anisotropy

The dielectric anisotropy is defined as $\Delta\varepsilon = \varepsilon_{//} - \varepsilon_{\perp}$, where $\varepsilon_{//}$ and $\varepsilon_{\perp}$ denote the dielectric permittivity parallel and perpendicular to the director, respectively. In notebook PC and other applications, low power consumption is critical. Thus, 3.3V and even 2.5V driving voltage are considered for TFT-LCDs. Therefore, high dielectric anisotropy LC-materials are attractive for low operating voltage.

From the molecular point of view, the origin of the dielectric anisotropy is the anisotropic distribution of the molecular dipoles in the liquid crystal phases. Therefore, nematic phases formed by elongated molecules carrying longitudinal and transverse dipoles have respectively positive and negative dielectric anisotropy, whose magnitude increases with that of the molecular dipoles and with the degree of ordering. Some software i.e. MOPAC [46] can be used to compute the molecular properties (such as dipole moment) before synthesis.

Maier and Meier [47] extended Onsager theory to nematic LC. In their theory, a molecule is represented by an anisotropic polarizability α with principal elements α_l and α_t in spherical cavity of radius a. Denoting the dipole moment with α_l at an angle θ, the LC dielectric components $\varepsilon_{//}$, $\varepsilon_{\perp}$ and $\Delta\varepsilon$ can be expressed as:

$$\varepsilon_{ll} = NhF\left\{\left\langle \alpha_{ll} \right\rangle + (F\mu^2 / 3kT)\left[1 - (1 - 3\cos^2\theta)S\right]\right\}, \tag{2.14}$$

$$\varepsilon_{\perp} = NhF\left\{\left\langle \alpha_{\perp} \right\rangle + (F\mu^2 / 3kT)\left[1 + (1 - 3\cos^2\theta)S / 2\right]\right\}, \tag{2.15}$$

$$\Delta\varepsilon = NhFS\left\{(\alpha_l - \alpha_t) - (F\mu^2 / 2kT)\left(1 - 3\cos^2\theta\right)\right\}, \tag{2.16}$$

where N is the molecular packing density, μ is the dipole moment, F is the Onsager reaction field and $\langle n \rangle$ is average refractive index. Here h and F are dependent on the average dielectric constant $\langle \varepsilon \rangle$ and average refractive index $\langle n \rangle$:

$$h = \frac{3\langle \varepsilon \rangle}{2\langle \varepsilon \rangle + 1}, \tag{2.17}$$

$$F = \frac{\left(2\langle \varepsilon \rangle + 1\right)\left(\langle n \rangle^2 + 2\right)}{3(2\langle \varepsilon \rangle + \langle n \rangle^2)}. \tag{2.18}$$

Based on Eq. (2.16), the dielectric anisotropic of an LC material is influenced by three factors: molecular structure, temperature, and frequency. Let us discuss each factor separately.

2.2.2.1 Molecular Structure Effect

For a non-polar linear LC compound, its dipole moment $\mu \sim 0$, thus its dielectric anisotropic $\Delta\varepsilon$ is small. For a polar LC compound with a polar group, e.g., cyano or fluoro, its Δε can be positive or negative depending on the positions of the polar groups. When $\theta < 55^\circ$, the dipole contribution to $\Delta\varepsilon$ is positive, while when $\theta > 55^\circ$ it is negative, as illustrated in Eq.(2.16). The sign of the dielectric anisotropy $\Delta\varepsilon$ will affect the molecular alignment. Positive $\Delta\varepsilon$ material tends to align parallel to the electric field, which negative one normal to the electric field. Most discotic shaped molecules have negative $\Delta\varepsilon$.

In order to measure either $\varepsilon_{//}$ or $\varepsilon_{\perp}$, capacitance method is commonly used. It is achieved by keeping the electric field parallel or perpendicular to the director with ac excitation at low frequency (normally 1 kHz). Two-cell method or one-cell at two voltages approach can both be used.

To increase $\Delta\varepsilon$, more than one polar group can be considered. The final $\Delta\varepsilon$ value is determined by the vector sum of the total dipole moments. The magnitude of $\Delta\varepsilon$ and polar group type of an LC mixture will affect the threshold voltage, operating voltage, power consumption, resistivity, and viscosity.

2.2.2.2 Temperature Effect

The temperature dependence of $\Delta\varepsilon$ is proportional to the order parameter S. Usually as temperature increases, $\varepsilon_{//}$ decreases while $\varepsilon_{\perp}$ increases gradually, resulting in a decreased $\Delta\varepsilon$. As $T > T_c$, the isotropic state is reached and the dielectric anisotropy is vanished.

2.2.2.3 Frequency Effect

Frequency dependent dielectric constant is another important factor in anisotropic LC material. At low frequency, $\Delta\varepsilon > 0$, while at high frequency, $\Delta\varepsilon$ could become negative. As f increases, $\varepsilon_{//}$ decreases while $\varepsilon_{\perp}$ stays constant, which results in a decreased $\Delta\varepsilon$. The dielectric anisotropy $\Delta\varepsilon$ changes its sign at the crossed frequency f_c. For a pure LC compound, its f_c is usually higher than 10 MHz, which is too high to be employed. Dual-frequency effect is a useful approach for achieving fast response time. However, the DFLC often exhibit a small $\Delta\varepsilon$ (i.e.,

high voltage) and high viscosity, and its crossover frequency is too sensitive to the operating temperature. These issues limit the widespread applications of DFLC materials.

2.2.3 Visco-elastic Properties

High birefringence is not the solely consideration of LC material, we need to account the overall performance, which is the Figure of Merit (FoM). Thus, another important parameter, visco-elastic coefficient, needs to be introduced, which is related to viscosity and elastic constants characteristics. Each factor will be analyzed in detail.

2.2.2.1 Elastic Constants

The free volume elastic energy (Frank energy) density of a nematic liquid crystal is written as:

$$f_{elastic} = \frac{1}{2}K_{11}(\nabla \cdot \vec{n})^2 + \frac{1}{2}K_{22}(\vec{n} \cdot \nabla \times \vec{n})^2 + \frac{1}{2}K_{33}(\vec{n} \cdot \nabla \cdot \vec{n})^2, \tag{2.19}$$

where K_{11}, K_{22}, and K_{33} are the elastic constants associated with spray, twist, and bend deformation, as shown in Figure 5, respectively.

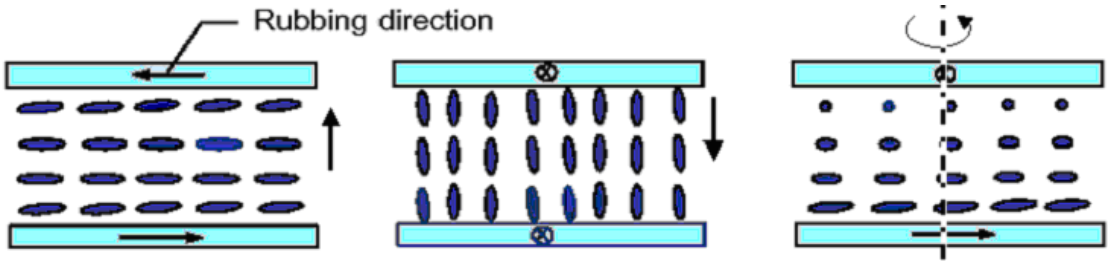

a) Splay (Homogeneous) b) Bend (homeotropic) c) Twist (twisted cell)

Figure 5: Demonstrations of three basic deformations of LC.

Each of them relates to a specific alignment of the LC cell, in that K_{11} for homogeneous cell, K_{22} for twisted nematic cell, and K_{33} for homeotropic cell. From Maier-Saupe theory, the elastic constants are linearly proportional to S^2 as:

$$K_{33} > K_{11} > K_{22} \sim S^2 . \tag{2.20}$$

A small elastic constant is favorable to achieve a low operation voltage, but it leads to a slow response time because the response time is proportional to $1/K_{ii}$. In practical uses, response time and viewing angle are usually more important than threshold voltage. Thus, multi-domain vertical alignment is a favorable approach for LCD TVs.

2.2.2.3 Rotational Viscosity

For almost all LC-related applications, fast response time is critical issue. Therefore, low viscosity LC materials are essential for TFT-LCDs. Rotational viscosity γ_1 plays a critical role to LC dynamics. Both rise time and decay time are linearly proportional to γ_1. Thus, for most LC devices, low rotational viscosity γ_1 LC material is favorable. The temperature-dependent rotational viscosity could be written as [29]:

$$\gamma_1 = bS \exp(E / k_0 T), \tag{2.21}$$

where E is the activation energy, T is the Kelvin temperature and S is the order parameter shown in Eq. (2.9). From the molecular standpoint, the rotational viscosity depends on the molecular constituents, dimensions, molecular interactions, and moment of inertia. Thus, a linearly conjugated liquid crystal should exhibit a relatively low rotational viscosity. At the elevated temperature, γ_1 decreases dramatically. For every 10°C temperature increase, viscosity is

decreased by ~2X.

Low viscosity and high resistivity are essential for TFT-LCDs where the LC birefringence is about 0.1. The commonly used molecular structures are fluorinated cyclohexane-phenyl (CP) two-ring and CCP three-ring compounds. Using a low viscosity LC mixture or operating a LC mixture at an elevated temperature, a small visco-elastic coefficient can be obtained. As a consequence, response time is reduced.

2.2.2.4 Figure of Merit

To characterize the overall performance of LC materials, a figure-of-merit (FoM) which takes birefringence and response time into account has been defined as [29]:

$$FoM = \frac{\Delta n^2}{\gamma_1 / K_{11}}, \tag{2.22}$$

where K_{11} is the splay elastic constant, Δn is the birefringence, γ_1 is the rotational viscosity. All of these parameters are temperature dependent. Both viscosity and elastic constants are also dependent on the order parameter S and can be approximated as:

$$\Delta n = (\Delta n)_0 S, \tag{2.23}$$

$$K_{ii} = aS^2. \tag{2.24}$$

Substituting Eqs. (2.21)-(2.24) into Eq.(2.22), the temperature dependent FoM is derived as:

$$FoM = (a/b)(\Delta n_0)^2 (1 - T/T_c)^{3\beta} \exp(-E/k_0 T), \tag{2.25}$$

where Δn_0 is the birefringence at S =1, E is activation energy of the liquid crystal and k_0 is the Boltzmann constant. The value of the β parameter is around 0.25 and insensitive to liquid crystal structures.

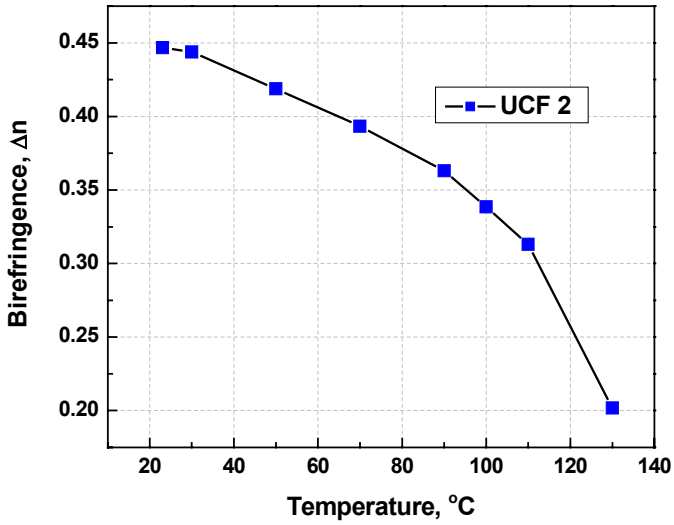

Figure 6: Temperature-dependent birefringence of UCF-2. Blue dots are experimental data at λ =633 nm.

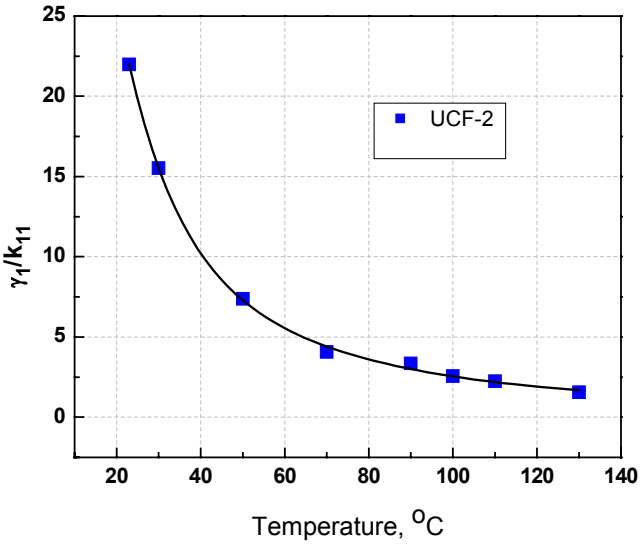

Figure 7: Temperature-dependent visco-elastic coefficient γ_1/k_{11} of UCF-2. Blue dots are experimental data.

Figure 6 shows the temperature dependent birefringence of UCF-2 at λ =633 nm. The nematic range of UCF-2 is from 10.3°C to 141°C. As the temperature increases, the birefringence decreases gradually. Figure 7 gives the visco-elastic coefficient of UCF-2. As can be seen from the figure, γ_1/k_{11} decreases as the temperature increases. When the temperature increases from T =23°C to T =70°C, the visco-elastic coefficient drops from γ_1/k_{11}= 22 to 4. Since LC switching time is proportional to γ_1/k_{11}, as a result, a fast response time is achieved by the reduced visco-elastic coefficient at an elevated temperature.

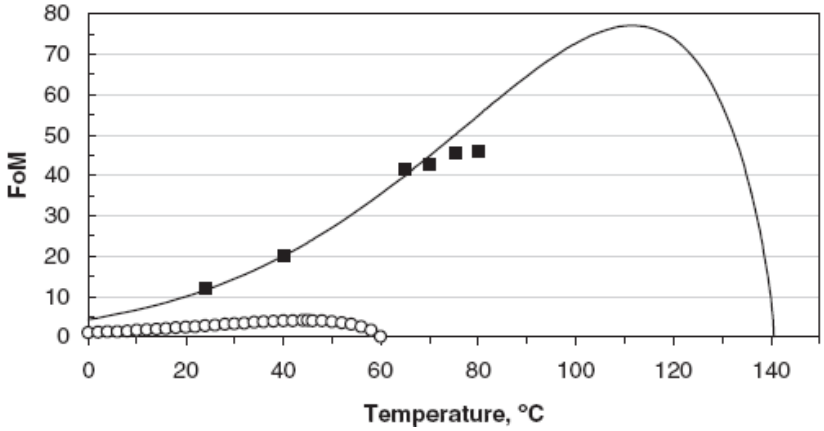

Figure 8: Temperature dependent figure-of-merit of UCF-2 (squares) and E7 (circles). Solid lines are fittings to the experimental data of UCF-2 using E =340 meV, β=0.25, and T_c =141°C at λ = 633 nm.

From above discussions, it can be seen that elastic constant, viscosity and birefringence are all dependent on temperature. Accordingly, the figure of merit strongly depends on the temperature. The temperature-dependent figure of merit for UCF-2 is depicted in Figure 8. At low-temperature region, even though birefringence, dielectric anisotropy, elastic constants and viscosity all reduce as temperature increases, the dropping speed of visco-elastic coefficient in

Figure 7 is faster than that of Δn^2. Therefore the figure of merit first increases with increasing temperature and reaches a maximum value at ~115°C. As the temperature approaches the clearing temperature T_c, birefringence has very steep drop as shown in Figure 6, which causes a sharp decrease in the figure of merit. The higher figure of merit a LC possesses, the faster response time it exhibits. Thus operating a LC device at an elevated temperature is beneficial for reducing response time. However, it brings complication to the driving scheme by the additional temperature control system. Also included in Figure 8 for comparison is a commercial E7 mixture. At 70°C, the UCF-2 mixture has 10X higher FoM than that of E7 at 48°C.

2.3 Anchoring Energy

The structure of liquid crystal directors in close proximity to an interface is different from that in the bulk, and this surface structure changes boundary conditions and influences the behavior of the LC director in the bulk. Therefore, the anchoring energy is an important parameter for a LC cell. It affects not only the LC alignment but also the electro-optic properties such as threshold voltage and response time.

The anchoring energy depends on cell thickness. A thinner cell exhibits a higher anchoring energy.

In contrast to the strong anchoring energy, weak anchoring can results in: 1) Lower threshold, 2) Rise time decreases, and 3) Fall time increases

2.4 Factors Affecting LC Response Time

To summarize the above discussions, we find that the LC response time depends on several factors, including the LC layer thickness, viscosity, temperature and surface treatment, as well as the driving waveform. The pretilt angle effect will be numerically analyzed in Sec. 4.3.1 in detail. The effects of these factors on the response time are listed in Table 1.

Table 1: The effects of different factors on response time

Factors	T_{rise}	T_{decay}
Viscosity (γ_1) ↓	↓	↓
Elastic constants (K_{ii}) ↑	↑	↓
Dielectric anisotropy ($\Delta\varepsilon$)↑	↓	↓
Thickness (d) ↓	↓	↓
Pretilt angle (θ_0) ↓	↑	↓
Anchoring energy (W) ↑	↑	↓
Temperature (T) ↑	↓	↓
Voltage (V) ↑	↓	↓

To achieve a fast response time, low rotational viscosity (γ_1) LC mixtures are preferred [16],[49]. Another straightforward approach is to use a thin cell gap filled with a high birefringence (Δn) and low viscosity LC mixture [36],[50]. High birefringence also enhances the display brightness and contrast ratio of polymer-dispersed liquid crystal (PDLC) [33],[34], holographic PDLC [35], cholesteric LCD [14],[31], and LC gels [51]-[53]. Recently, many manufacturers have reported the display devices with reduced cell gaps of below 4 μm in order to achieve fast response time.

CHAPTER 3: SIMULATION METHODOLOGIES

Numerical simulation is an important tool in the design and optimization of liquid crystal (LC) devices with high quality performance, which includes fast response time and wide viewing angle. In this chapter, we will review recent development of LCD modeling methods.

In general, the modeling of liquid crystal devices can be divided into two steps: (1) find director distribution; and (2) simulate optical response.

3.1 Simulation of Director Distribution

For a homogeneous LC cell that is strong anchored at the surface of z_1=0 and z_2=d with a small pretilt angle (~3°) to the normal, when no voltage is applied, the LC molecules are parallel to the electrodes except a small pretilt angle to avoid reverse tilt disclination. When the applied voltage exceeds Freedericksz transition voltage V_{th}, the LC molecules will rotate and be reoriented by the electric field, causing the change of the permittivity of substrate.

The director distribution under applied voltage of LC devices should be solved first. Whether the backflow effect should be considered depends on the applied voltage. Thus we divide it into two categories: without or with backflow effect.

3.1.1 Without Backflow Effect

Under the circumstance when backflow effect is not considered, two-step approach is used: solve the voltage distribution using the finite element method (FEM) [54], and then obtain the director distribution using the finite difference method (FDM) [55].

The steady-state LC director distribution is controlled by the balance of the torques

between the elastic free energy and electric energy. The electric energy under applied voltage is defined as [56]:

$$f_{Electric} = \iiint \left(\frac{1}{2} D \cdot E \right) dv = \iiint \left(\frac{1}{2} \varepsilon \nabla V \cdot \nabla V \right) dv \,. \tag{3.1}$$

where V is the voltage distribution, and ε is the dielectric tensor of the LC cell. The relative dielectric tensor of the LC cell is given by [57]:

$$\boldsymbol{\varepsilon}_r = \begin{bmatrix} \varepsilon_{xx} & \varepsilon_{xy} & \varepsilon_{xz} \\ \varepsilon_{yx} & \varepsilon_{yy} & \varepsilon_{yz} \\ \varepsilon_{zx} & \varepsilon_{zy} & \varepsilon_{zz} \end{bmatrix}, \tag{3.2}$$

where

$$\varepsilon_{xx} = n_o^2 + (n_e^2 - n_o^2)\cos^2\theta\cos^2\phi, \tag{3.3}$$

$$\varepsilon_{yy} = n_o^2 + (n_e^2 - n_o^2)\cos^2\theta\sin^2\phi, \tag{3.4}$$

$$\varepsilon_{zz} = n_o^2 + (n_e^2 - n_o^2)\sin^2\theta, \tag{3.5}$$

$$\varepsilon_{yz} = \varepsilon_{zy} = (n_e^2 - n_o^2)\sin\theta\cos\theta\sin\phi, \tag{3.6}$$

$$\varepsilon_{xy} = \varepsilon_{yx} = (n_e^2 - n_o^2)\cos^2\theta\sin\phi\cos\phi, \tag{3.7}$$

$$\varepsilon_{xz} = \varepsilon_{zx} = (n_e^2 - n_0^2)\sin\theta\cos\theta\cos\phi, \tag{3.8}$$

Here, n_o and n_e is the ordinary and extraordinary refractive indices of the LC medium, respectively, θ is the tilt angle of the LC director, which is the angle between the LC director and the x-y plane, and ϕ is the azimuthal angle between projection of the LC director on the x-y plane and the x-axis as shown in Figure 9.

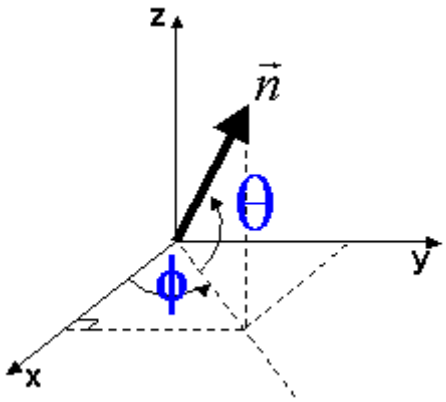

Figure 9: The coordinate system of LC director.

Using rectangular elements, the voltage distribution can be expressed as a set of linear equations [57]:

$$V(x,y,z)=\sum_{e=1}^{Ne}\sum_{i}V_i^e N_i^e(x,y,z), \tag{3.9}$$

where V_i^e is the unknown voltage at the node i of element e, N_e is the total number of elements, and $N_i^e(x,y,z)$ is the shape function.

To minimize this functional, the variation of the electric energy $F_{Electric}$ on the voltage V_m of node m is equal to 0. After solving the following linear algebraic equation [56], the voltage distribution is obtained.

$$\begin{pmatrix} A_{11} & A_{12} & \cdots & A_{1N_{node}} \\ A_{21} & A_{22} & \cdots & A_{2N_{node}} \\ \vdots & \vdots & \ddots & \vdots \\ A_{N_{node}1} & A_{N_{node}2} & \cdots & A_{N_{node}N_{node}} \end{pmatrix} \begin{pmatrix} V_1 \\ V_2 \\ \\ V_{N_{node}} \end{pmatrix} = 0, \tag{3.10}$$

where

$$A_{mn} = \frac{\partial^2 F^e_{Electric}}{\partial V_m \partial V_n}. \tag{3.11}$$

In the following, we will discuss the solution of director distribution.

The main idea is to use Euler-Lagrangian equations to minimize the free energy. After applying the Gibbs free-energy density f_g to the Erickson-Leslie theory, we have [59]:

$$\gamma_1 \frac{dn_i}{dt} = -\left[f_g\right]_{n_i} + \lambda n_i, \quad i = x, y, z \tag{3.12}$$

where γ_1 is the rotational viscosity, n_i is Cartesian component of the director, λ is a Lagrange multiplier used to maintain the unit length of the director and $[f_g]_{ni}$ is the Euler-Lagrangian equations. However, it is impossible to solve for both an update formula for the director and λ, so we drop the Lagrange multiplier term and simply renormalize the director after each iteration. The Euler-Lagrangian equations $[f_g]_{ni}$ are expressed as [59]:

$$\left[f_g\right]_{n_i} = \frac{\partial f_g}{\partial n_i} - \frac{d}{dx}\left(\frac{\partial f_g}{\partial n_i / dx}\right) - \frac{d}{dy}\left(\frac{\partial f_g}{\partial n_i / dy}\right) - \frac{d}{dz}\left(\frac{\partial f_g}{\partial n_i / dz}\right), \quad i = x, y, z \tag{3.13}$$

where f_g is the Gibbs free energy density given by:

$$f_g = f_{elastic} - f_{Electric}. \tag{3.14}$$

Here $f_{elastic}$ and $f_{Electric}$ are the elastic free energy density and electric energy density, as expressed in Eqs. (2.19) and (3.1), respectively.

With the known electric energy density $f_{Electric}$ and elastic energy density $f_{elastic}$, the updated director components after each time step Δt can be derived from equation Eq. (3.12) as

$$n_i^{new} = n_i^{old} - \frac{\Delta t}{\gamma_1}\left[f_g\right]_{n_i}, i = x, y, z. \tag{3.15}$$

After this update, the director must be renormalized to have a unit length. This renormalization also depends on the numerical time step Δt. Therefore, the setting time step will be critical to the calculation accuracy. In our simulation, we use a flexible time step Δt, which is less than the maximum time step given by [59]:

$$\Delta t_{\max} = \frac{\Delta x^2 \gamma_1}{2k_{11}}, \tag{3.16}$$

where Δx is the minimum meshing size of the x, y, z direction. At each time step, the director distribution is visualized, which will be used to solve the electro-optical performance of the simulated LC device. After the LC director distribution is updated, the voltage distribution and the electric energy distribution must be updated to represent the changes of the voltage distribution. This iteration continues until setting convergence criteria is reached. This is a good approach in reducing the computation time while maintaining a reasonable accuracy.

3.1.2 With Backflow Effect

When backflow effect is considered, another step should be added in the director update using finite difference method. The director is therefore under the tilt deformation, associated with the viscous torque. In the Cartesian coordinate, the director is fully described as $\mathbf{n} = (n_x, n_y, n_z)$, the director distribution in 1-D case will follow the rule as:

$$\gamma_1 \dot{n}_x = \gamma m_x - \frac{\partial F}{\partial n_x} + \frac{\partial}{\partial z}\frac{\partial F}{\partial n_{x,z}} - \alpha_2 n_z \frac{\partial v_x}{\partial z}, \tag{3.17}$$

$$\gamma_1 \dot{n}_y = \gamma m_y - \frac{\partial F}{\partial n_y} + \frac{\partial}{\partial z}\frac{\partial F}{\partial n_{y,z}} - \alpha_2 n_z \frac{\partial v_y}{\partial z}, \tag{3.18}$$

$$\gamma_1 \dot{n}_z = \gamma n_z - \frac{\partial F}{\partial n_z} + \frac{\partial}{\partial z}\frac{\partial F}{\partial n_{z,z}} + \varepsilon_0 \Delta\varepsilon E^2 n_z - \alpha_3 n_x \frac{\partial v_x}{\partial z} - \alpha_3 n_y \frac{\partial v_y}{\partial z}, \tag{3.19}$$

where F is the Frank free energy density, γ_1 is the rotational viscosity, $\dot{n}_x, \dot{n}_y$, and $\dot{n}_z$ are the differential of n_x, n_y, n_z to time t, and v_x, v_y are flow velocity along x and y direction. Notice the inertial terms have been neglected in the director equation. The last terms in the above equations are related to the viscous torque. So we have another two parameters need to be solved first: $\frac{\partial v_x}{\partial z}$ and $\frac{\partial v_y}{\partial z}$, which are given by the following two flow equations:

$$\rho \dot{v}_x = \frac{\partial}{\partial z}\left[\alpha_2 \dot{n}_x n_z + \alpha_3 \dot{n}_x n_x + \frac{1}{2}\alpha_3 n_x n_y \frac{\partial v_y}{\partial z} + \frac{1}{2}(2\alpha_1 n_x^2 n_z^2 + (\alpha_5 - \alpha_2) n_z^2 + \alpha_4 + (\alpha_3 + \alpha_6) n_x^2)\frac{\partial v_x}{\partial z}\right], \tag{3.20}$$

$$\rho \dot{v}_y = \frac{\partial}{\partial z}\left[\alpha_2 \dot{n}_y n_z + \alpha_3 \dot{n}_z n_y + \frac{1}{2}\alpha_3 n_x n_y \frac{\partial v_x}{\partial z} + \frac{1}{2}(2\alpha_1 n_y^2 n_z^2 + (\alpha_5 - \alpha_2) n_z^2 + \alpha_4 + (\alpha_3 + \alpha_6) n_y^2)\frac{\partial v_y}{\partial z}\right]. \tag{3.21}$$

where α_1 to α_6 are six Leslie coefficients, and ρ is the fluid density. Because the inertia is small, and can be omitted, the following equations are derived:

$$\frac{1}{2}\alpha_3 n_x n_y \frac{\partial v_y}{\partial z} + \frac{1}{2}(2\alpha_1 n_x^2 n_z^2 + (\alpha_5 - \alpha_2) n_z^2 + \alpha_4 + (\alpha_3 + \alpha_6) n_x^2)\frac{\partial v_x}{\partial z} = C_1 - \alpha_2 \dot{n}_x n_z - \alpha_3 \dot{n}_z n_x, \tag{3.22}$$

$$\frac{1}{2}\alpha_3 n_x n_y \frac{\partial v_x}{\partial z} + \frac{1}{2}(2\alpha_1 n_y^2 n_z^2 + (\alpha_5 - \alpha_2) n_z^2 + \alpha_4 + (\alpha_3 + \alpha_6) n_y^2)\frac{\partial v_y}{\partial z} = C_2 - \alpha_2 \dot{n}_y n_z - \alpha_3 \dot{n}_z n_y. \tag{3.23}$$

To get the solutions of $\frac{\partial v_x}{\partial z}$ and $\frac{\partial v_y}{\partial z}$, we need to find the C_1, C_2 first. With the boundary condition $\frac{\partial v_x}{\partial z} = \frac{\partial v_y}{\partial z} = 0$ at z =0 and d, and the director distribution (n_x, n_y, n_z) at time step (i), we can obtain the solutions of C_1, C_2. After that, the values of $\frac{\partial v_x}{\partial z}$ and $\frac{\partial v_y}{\partial z}$, can be obtained from Eqs.(3.22) and (3.23). Substituting them into Eqs. (3.17)-(3.19), the updated director distribution (n_x', n_y', n_z') at this time step (i) is obtained. Using our in-house developed program, the dynamics of LC cells with backflow effect is investigated and the results will be explored in Chapter 5.

3.2 Optical Simulation

In this section, two commonly employed approaches for calculating the transmittance is introduced: 1) the 4 by 4 matrix method [61]-[64], 2) the extended Jones matrix (2 by 2 matrix) [65]-[69]. Berreman's 4×4 Matrix approach takes into account the effects of the refraction and multiple reflections between adjacent plate interfaces [62]. However, it needs lengthy calculations and it is generally employed only for the normal incidence. Over these years many approximations to this scheme has been proposed. Yeh [65] and Lien's [67] extended Jones matrix methods were derived to generalize the 4×4 Matrix formulation to the oblique incidence. Huang et al. [69] used an improved 4×4 Matrix for optimizing the liquid crystal Fabry-Perot etalon for telecom application.

3.2.1 4×4 Matrix Method

Let us consider an unpolarized light entering a LC panel at an oblique direction. We choose a coordinate system in which the wave vector **k** of the incident plane wave lies in the *x*-*z* plane. Here the +*z* axis points from the bottom glass substrate to the exit polarizer. The wave vector of the incident wave in this coordinate system is given by

$$\mathbf{k}_{\mathbf{in}} = \mathbf{x}k_0 \sin\theta_k + \mathbf{y}\cdot 0 + \mathbf{z}k_o \cos\theta_k, \tag{3.24}$$

where k_0 is the wave number in free space, θ_k is elevation angle of the incident plane wave, and **x**, **y**, and **z** are the unit vector in the *x*, *y*, *z* directions, respectively. The whole LCD system is divided into *N* layers in the *z* direction. *N* is normally a number less than 100 such that each layer is considered as a homogeneous one. The liquid crystal layer shown in the figure usually consists of 30-50 layers. In simulations, each layer is treated as a single homogenous one.

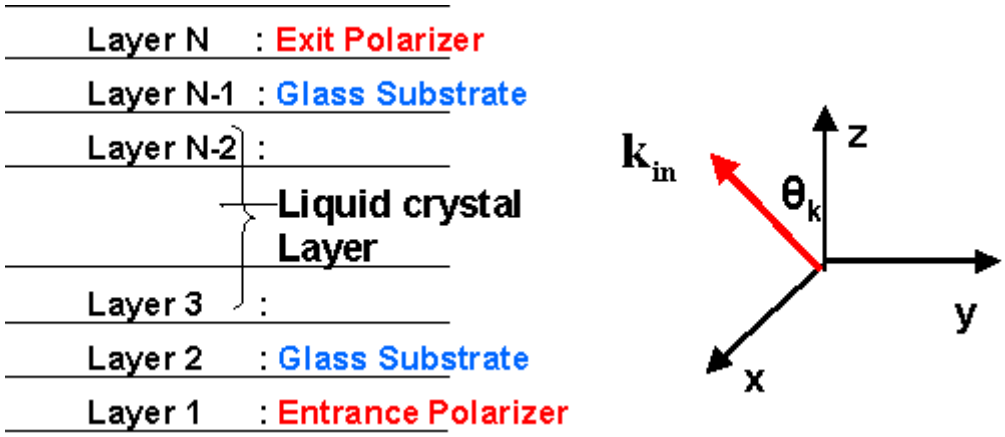

Figure 10: Schematic diagram of a LC panel, which is divided into N layers.

For simplicity, the magnetic field intensity $\mathbf{H}$ is normalized as:

$$\hat{\mathbf{H}} = \left(\frac{\mu_0}{\varepsilon_0}\right)^{1/2} \mathbf{H} \tag{3.25}$$

Assuming **E** and $\hat{\mathbf{H}}$ are *exp(-iwt)* dependent, the time harmonic Maxwell equation can be expressed as:

$$\nabla \times \mathbf{E} = ik_o \hat{\mathbf{H}}, \tag{3.26}$$

$$\nabla \times \hat{\mathbf{H}} = -ik_o \bar{\varepsilon} \mathbf{E}. \tag{3.27}$$

With $\partial / \partial y = 0$ and $\partial / \partial x = ik_x$, after expansion of Maxwell's equations, we can derive the following form:

$$\frac{\partial}{\partial z}\begin{pmatrix} E_x \\ E_y \\ \hat{H}_x \\ \hat{H}_y \end{pmatrix} = ik_0 \mathbf{Q} \begin{pmatrix} E_x \\ E_y \\ \hat{H}_x \\ \hat{H}_y \end{pmatrix}, \tag{3.28}$$

where **Q** is a coupling matrix given by

$$\mathbf{Q} = \begin{bmatrix} -\frac{\varepsilon_{zx}}{\varepsilon_{zz}}\sin\theta_k & -\frac{\varepsilon_{zy}}{\varepsilon_{zz}}\sin\theta_k & 0 & 1-\frac{\sin^2\theta_k}{\varepsilon_{zz}} \\ 0 & 0 & -1 & 0 \\ -\varepsilon_{yx}+\varepsilon_{yz}\frac{\varepsilon_{zx}}{\varepsilon_{zz}} & -\varepsilon_{yy}+\varepsilon_{yz}\frac{\varepsilon_{zy}}{\varepsilon_{zz}}+\sin^2\theta_k & 0 & \frac{\varepsilon_{yz}}{\varepsilon_{zz}}\sin\theta_k \\ \varepsilon_{xx}-\varepsilon_{xz}\frac{\varepsilon_{zx}}{\varepsilon_{zz}} & \varepsilon_{xy}-\varepsilon_{xz}\frac{\varepsilon_{zy}}{\varepsilon_{zz}} & 0 & -\frac{\varepsilon_{xz}}{\varepsilon_{zz}}\sin\theta_k \end{bmatrix}. \tag{3.29}$$

For each sub-layer, the matrix **Q** can be transformed to a diagonalized matrix:

$$\mathbf{Q} = \mathbf{T}\begin{bmatrix} q_1 & & & \\ & q_2 & & \\ & & q_3 & \\ & & & q_4 \end{bmatrix}\mathbf{T}^{-1}, \tag{3.30}$$

where q_1 to q_4 are the four eigenvalues, and **T** is composed of the corresponding eigenvectors. q_1 to q_4 are given by

$$q_1 = \left(n_o^2 - \sin^2\theta_k\right)^{1/2}, \tag{3.31}$$

$$q_2 = -\frac{\varepsilon_{xz}}{\varepsilon_{zz}}\sin\theta_k + \frac{n_o n_e}{\varepsilon_{zz}}\left[\varepsilon_{zz} - \left(1 - \frac{n_e^2 - n_o^2}{n_e^2}\cos^2\theta\sin^2\varphi\right)\sin^2\theta_k\right]^{1/2}, \tag{3.32}$$

$$q_3 = -q_1, \tag{3.33}$$

$$q_4 = -q_2, \tag{3.34}$$

where q_1 and q_2 correspond to two forward eigenwaves, and q_3 and q_4 correspond to two backward eigenwaves.

With the diagonalized **Q** matrix, we can further conduct a variable transformation of the tangential field components as:

$$\begin{bmatrix} E_x \\ E_y \\ \widehat{H}_x \\ \widehat{H}_y \end{bmatrix} = \mathbf{T}\begin{bmatrix} U_1 \\ U_2 \\ U_3 \\ U_4 \end{bmatrix}. \tag{3.35}$$

where **T** is expanded as:

$$\mathbf{T} = \begin{bmatrix} T_{11} & T_{12} \\ T_{21} & T_{22} \end{bmatrix}. \tag{3.36}$$

Substituting Eqs. (3.30) and (3.35) into Eq. (3.28), we have the decoupled equations as:

$$\frac{\partial}{\partial z}\begin{bmatrix} U_1 \\ U_2 \\ U_3 \\ U_4 \end{bmatrix} = ik_0\begin{bmatrix} q_1 & & & \\ & q_2 & & \\ & & q_3 & \\ & & & q_4 \end{bmatrix}\begin{bmatrix} U_1 \\ U_2 \\ U_3 \\ U_4 \end{bmatrix}. \tag{3.37}$$

For the n^{th} sub-layer, the solution of Eq. (3.37) is given by:

$$\begin{bmatrix} U_1 \\ U_2 \\ U_3 \\ U_4 \end{bmatrix}_{n,d_n} = \mathbf{H_n} \begin{bmatrix} U_1 \\ U_2 \\ U_3 \\ U_4 \end{bmatrix}_{n,0}, \tag{3.38}$$

where $\begin{bmatrix} U_1 \\ U_2 \\ U_3 \\ U_4 \end{bmatrix}_{n,0}$ and $\begin{bmatrix} U_1 \\ U_2 \\ U_3 \\ U_4 \end{bmatrix}_{n,d_n}$ are the eigenwaves on the input and output boundaries of the n^{th} sub-layer , respectively and d_n is the thickness of the corresponding n^{th} layer, The matrix $\mathbf{H_n}$ is

$$\mathbf{H_n} = \begin{bmatrix} \exp(ik_{z_1} d_n) & & & \\ & \exp(ik_{z_2} d_n) & & \\ & & \exp(ik_{z_3} d_n) & \\ & & & \exp(ik_{z_{41}} d_n) \end{bmatrix}, \tag{3.39}$$

where

$$k_{z_1} = k_0 q_1, \tag{3.40}$$

$$k_{z_2} = k_0 q_2, \tag{3.41}$$

$$k_{z_3} = k_0 q_3, \tag{3.42}$$

$$k_{z_4} = k_0 q_4. \tag{3.43}$$

Substituting Eq. (3.38) into Eq. (3.35), the electric field on the output boundary of the n^{th} layer is related to the electric field on the input boundary of the same layer by

$$\begin{bmatrix} E_x \\ E_y \\ \widehat{H}_x \\ \widehat{H}_y \end{bmatrix}_{n,d_n} = \mathbf{P_n} \begin{bmatrix} E_x \\ E_y \\ \widehat{H}_x \\ \widehat{H}_y \end{bmatrix}_{n,0}, \tag{3.44}$$

where $\mathbf{P_n}$ is the 4-by-4 matrix of the n^{th} sub-layer and is given by

$$\mathbf{P_n} = \mathbf{T_n H_n T}_n^{-1}. \tag{3.45}$$

Since the tangential **E** field components are continuous in the interfaces of adjacent layers, the 4-by-4 matrix of the simulated LC device can be expressed as:

$$\mathbf{P} = \mathbf{P_N P_{N-1}} \dots \mathbf{P_2 P_1}. \tag{3.46}$$

3.2.2 2×2 Matrix or Extended Jones Matrix Method

If we assume the reflection inside the LC device is negligible and only consider the forward eigenwaves, Eq. (3.35) becomes:

$$\begin{bmatrix} E_x \\ E_y \end{bmatrix} = \mathbf{T_{11}} \begin{bmatrix} U_1 \\ U_2 \end{bmatrix} = \mathbf{S} \begin{bmatrix} U_1 \\ U_2 \end{bmatrix}. \tag{3.47}$$

For the eigenwave in the nth layer, we have

$$\begin{bmatrix} U_1 \\ U_2 \end{bmatrix}_{n,d_n} = \mathbf{G_n} \begin{bmatrix} U_1 \\ U_2 \end{bmatrix}_{n,0}, \tag{3.48}$$

where

$$\mathbf{G_n} = \begin{bmatrix} \exp(ik_{z_1} d_n) & \\ & \exp(ik_{z_2} d_n) \end{bmatrix}. \tag{3.49}$$

Applying equation (3.47) to equation (3.46), the extended Jones matrix of the n^{th} layer is

$$\mathbf{J_n} = \mathbf{S_n G_n S_n}^{-1}, \tag{3.50}$$

from which we can obtain the extended Jones matrix of the simulated LC device as

$$\mathbf{J} = \mathbf{J_N J_{N-1}} \dots \mathbf{J_2 J_1}. \tag{3.51}$$

Considering the transmission loss in the air-LCD interface, the transmitted electric field is related to the incident electric field by:

$$\begin{bmatrix} E_x \\ E_y \end{bmatrix}_{N+1} = \mathbf{J}\begin{bmatrix} E_x \\ E_y \end{bmatrix}_1 = \mathbf{J_{Ext}}\mathbf{J_N}\mathbf{J_{N-1}}\cdots\mathbf{J_2}\mathbf{J_1}\mathbf{J_{Ent}}\begin{bmatrix} E_x \\ E_y \end{bmatrix}_1, \tag{3.52}$$

where $\mathbf{J_{Ext}}$ and $\mathbf{J_{Ent}}$ are the matrices considering the transmission losses in the air-LCD interfaces, which are given by

$$\mathbf{J_{Ent}} = \begin{bmatrix} \dfrac{2\cos\theta_p}{\cos\theta_p + n_p\cos\theta_k} & 0 \\ 0 & \dfrac{2\cos\theta_k}{\cos\theta_k + n_p\cos\theta_p} \end{bmatrix}, \tag{3.53}$$

$$\mathbf{J_{Ext}} = \begin{bmatrix} \dfrac{2n_p\cos\theta_k}{\cos\theta_p + n_p\cos\theta_k} & 0 \\ 0 & \dfrac{2n_p\cos\theta_p}{\cos\theta_k + n_p\cos\theta_p} \end{bmatrix}, \tag{3.54}$$

where n_p is the refraction index of the polarizer, and θ_p is given by

$$\theta_p = \sin^{-1}\left(\sin\theta_k / \mathrm{Re}\left(\frac{n_{e,p} + n_{o,p}}{2}\right)\right), \tag{3.55}$$

where $n_{e,p}$ and $n_{o,p}$ are the two refractive indices of the polarizer.

Thus, the overall optical transmittance t_{op} is given by

$$t_{op} = \frac{\left|E_{x,N+1}\right|^2 + \cos^2\theta_p\left|E_{y,N+1}\right|^2}{\left|E_{x,1}\right|^2 + \cos^2\theta_p\left|E_{y,1}\right|^2}. \tag{3.56}$$

CHAPTER 4: CORRELATIONS BETWEEN LIQUID CRYSTAL DIRECTOR REORIENTAION AND OPTICAL RESPONSE TIME OF A HOMEOTROPIC CELL

4.1 Introduction

Response time is one of the most critical issues for nearly all liquid crystal (LC) devices involving dynamic switching. Based on the small angle approximation, Jakeman and Raynes derived the LC *director* reorientation times [72]. Since then, numerous papers dealing with LC response time have been published, however, the response time formula that most literatures refer to is the LC *director* reorientation time rather than the *optical* response time. For amplitude modulation, e.g., liquid crystal display devices [32], the LC device is usually sandwiched between two polarizers. The measured quantity is transmittance change and the associated dynamic response is optical rise or decay time. On the other hand, for a phase-only modulator such as optical phased arrays [36], the measured response time is phase change. There is no doubt that the optical response time for amplitude modulation and phase response time for phase modulation must be related to the LC director reorientation time. To quantify a display device, the rise and decay time is usually defined as intensity change between 10% and 90%. However, the correlation between the director reorientation time and the optical and phase response time has not been carefully studied. Based on a simplified model, Wu [73] found that the optical decay time could be ~2X faster than the director reorientation time in a homogeneous LC cell. It is important to establish the detailed correlation between the LC director reorientation time and the optical and phase response time.

In this chapter, we derived the analytical correlation between the director reorientation time and its consequent optical rise and decay times based on the small angle approximation. A vertical-aligned (VA, also known as homeotropic, DAP cell) [74] nematic LC cell was used for these studies due to its simple electro-optic characteristics and widespread applications in transmissive direct-view and reflective projection displays [75]-[77]. In that situation, the incoming linearly polarized light with a wave vector *k* in parallel to the z axis does not encounter birefringence, and arrives at the second substrate with an unchanged state of its polarization, If the analyzer is crossed with the polarizer, the light is blocked at the output for all the wavelength and independent of *d*, This is the normally black state. To validate the derived correlations, in Sec. 4.2 we numerically solved the dynamic Erickson-Leslie equation. Results indicate that the optical response time is linearly proportional to the director reorientation time and is weakly dependent on the initial bias voltage. Pretilt angle effect is found to make an important contribution to the LC dynamics. Gray scale switching of the VA cell is also studied and results are discussed in Sec. 4.3.

4.2 Theory

When the backflow and inertial effects are ignored, the dynamics of the LC director reorientation is described by the following Erickson-Leslie equation [78],[79]:

$$(K_{11}\cos^2\phi + K_{33}\sin^2\phi)\frac{\partial^2\phi}{\partial z^2} + (K_{33} - K_{11})\sin\phi\cos\phi(\frac{\partial\phi}{\partial z})^2 + \varepsilon_o\Delta\varepsilon E^2\sin\phi\cos\phi = \gamma_1\frac{\partial\phi}{\partial t}, \tag{4.1}$$

where γ_1 is the rotational viscosity, K_{11} and K_{33} represent the splay and bend elastic constants, respectively, $\varepsilon_o\Delta\varepsilon E^2$ is the electric field energy density, $\Delta\varepsilon$ is the LC dielectric anisotropy, and ϕ

is the tilt angle of the LC directors. In general, Eq. (4.1) can only be solved numerically. However, when the tilt angle is small ($\sin\phi \sim \phi$) and K_{33}~K_{11} (so called small angle approximation) [72], the Erickson-Leslie equation is reduced to:

$$K_{33}\frac{\partial^2\phi}{\partial z^2} + \varepsilon_o \Delta\varepsilon E^2\phi = \gamma_1\frac{\partial\phi}{\partial t}. \tag{4.2}$$

Under such circumstances, both rise time and decay time have simple analytical solutions.

4.2.1 Decay Time

When the electric field is switched off, i.e., E=0, Eq. (4.2) is further simplified as:

$$K_{33}\frac{\partial^2\phi}{\partial z^2} = \gamma_1\frac{\partial\phi}{\partial t}. \tag{4.3}$$

The solution of Eq. (4.3) can be expressed as

$$\phi(z,t) \cong \phi_m \sin(\frac{\pi z}{d})\exp(-\frac{t}{\tau_o}), \tag{4.4}$$

with

$$\tau_o = \frac{\gamma_1 d^2}{K_{33}\pi^2}, \tag{4.5}$$

where ϕ_m is the maximum tilt angle of the LC directors in the response of the applied voltage, d is the LC cell gap, z is the position of the oriented LC layer under discussion, and τ_o is the LC director reorientation time (1→1/e). It should be pointed out that in the Erickson-Leslie equation the strong surface anchoring and zero pretilt angle at the surface boundaries are assumed. Under such conditions, the Freedericksz transition threshold exists [80]:

$$V_{th} = \pi \sqrt{\frac{K_{33}}{\varepsilon_o \Delta\varepsilon}}. \tag{4.6}$$

The time-dependent phase change associated with this angle change is described as follows:

$$\Delta(t) = \frac{2\pi}{\lambda} \int_0^d \left[\frac{n_e n_o}{(n_o^2 \cos^2 \phi + n_e^2 \sin^2 \phi)} - n_o \right] dz, \tag{4.7}$$

where n_e and n_o are the refractive indices for the extraordinary and ordinary rays, respectively. If a VA cell is initially biased at a voltage (V_b) which is not too far above V_{th}, and the voltage is removed instantaneously at t =0, the transient phase change can be approximated from Eq. (4.7) as [81]:

$$\delta(t) \cong \delta_o \exp(-\frac{2t}{\tau_o}), \tag{4.8}$$

where δ_o is the net phase change from V=V_b to V=0. From Eq. (4.8), the phase decay time constant (1→1/e) is $\tau_o / 2$ which is 2X faster than the LC reorientation time.

To find optical response time, we need to calculate the intensity change. The time-dependent normalized intensity change *I(t)* of the VA cell under crossed polarizers can be calculated using the following relationship:

$$I(t) = \sin^2(\frac{\delta(t)}{2}). \tag{4.9}$$

Substituting Eq. (4.8) into Eq. (4.9), we find

$$I(t) = \sin^2\left(\frac{\delta_o \exp(-\frac{2t}{\tau_o})}{2} \right). \tag{4.10}$$

In a display device, two definitions of response time are encountered: optical transmittance change from 90% to 10% or from 100% to 10%. The process for correlating the optical response time to the director reorientation time is similar. Let us consider the former case first.

Based on Eq. (4.10), the normalized transmittance at t =0 has the following simple expression:

$$I_o = \sin^2(\frac{\delta_o}{2}). \tag{4.11}$$

Let us assume from t_1 to t_2 the transmittance decays from I_1 = 90% to I_2 = 10%. From Eq. (4.10), I_1 and I_2 have the following forms:

$$I_1 = 0.9I_o = \sin^2\left(\frac{\delta_o \exp(-\frac{2t_1}{\tau_o})}{2}\right), \tag{4.12}$$

$$I_2 = 0.1I_o = \sin^2\left(\frac{\delta_o \exp(-\frac{2t_2}{\tau_o})}{2}\right). \tag{4.13}$$

Using Eqs. (4.11), (4.12), and (4.13), we can easily solve the optical decay time T_{decay} (90%→10%) as follows

$$T_{decay} = t_2 - t_1 = \frac{\tau_o}{2}\ln\left(\frac{\sin^{-1}\left(\sqrt{0.9}\sin(\frac{\delta_o}{2})\right)}{\sin^{-1}\left(\sqrt{0.1}\sin(\frac{\delta_o}{2})\right)}\right). \tag{4.14}$$

Equation (4.14) correlates the optical decay time to the LC director reorientation time (τ_o). Similarly, the optical decay time from 100% to 10% can be derived easily and result is shown below:

$$T_{decay} = t_1 = \frac{\tau_o}{2} \ln \left(\frac{\delta_o / 2}{\sin^{-1}\left(\sqrt{0.1} \sin(\frac{\delta_o}{2}) \right)} \right). \tag{4.15}$$

Based on Eqs. (4.14) and (4.15), the optical decay time of a VA cell is linearly proportional to the director decay time. The initial phase retardation (δ_o) also plays an important role, but not too substantially. The detailed numerical results will be shown in Sec. 4.3.

4.2.2 Rise Time

Rise time is much more complicated to deal with than relaxation. The original small angle approximation used by Jakeman and Raynes for rise time is oversimplified [72]. They have assumed that the LC director's tilt angle increases exponentially with time. This approximation is valid only in a very short time regime. Blinov has considered the second order term and the fact that the LC directors will eventually reach an equilibrium stage. Thus, Eq.(4.2) is rewritten as [82]:

$$\xi^2 \frac{\partial^2 \phi}{\partial z^2} + \phi - \frac{1}{2}\phi^3 = \lambda \frac{\partial \phi}{\partial t}, \tag{4.16}$$

where

$$\lambda = \frac{\gamma_1}{\varepsilon_o \Delta\varepsilon E^2}, \tag{4.17}$$

$$\xi^2 = \frac{K_{33}}{\varepsilon_o \Delta\varepsilon E^2}. \tag{4.18}$$

In Eqs. (4.17) and (4.18), the electric field intensity E is expressed as:

$$E = V / d, \tag{4.19}$$

where the bias voltage V should satisfy $(V\text{-}V_{th})/V_{th} \leq 1$. Under such a circumstance, the solution of Eq. (4.16) can be approximated as:

$$\phi = \phi_m(t) \sin(\frac{\pi z}{d}). \tag{4.20}$$

Substituting Eq. (4.20) to Eq. (4.16), we obtain:

$$\left[1 - \left(\frac{V_{th}}{V}\right)^2\right]\phi_m - \frac{\phi_m^3}{2} = \lambda \frac{d\phi_m}{dt}. \tag{4.21}$$

Equation (4.21) has following solution:

$$\phi_m^2 = \frac{\phi_\infty^2}{1 + \left[\frac{\phi_\infty^2}{\phi_o^2} - 1\right]\exp\left(-\frac{2t}{\tau_r}\right)}, \tag{4.22}$$

where $\phi_\infty = \phi(t \to \infty)$ is the steady-state value of ϕ_m corresponding to the biased voltage, $\phi_o = \phi(t = 0)$ is the initial directors fluctuation, and τ_r is the directors rise time:

$$\tau_r = \frac{\gamma_1}{\left|\varepsilon_o |\Delta\varepsilon| E^2 - \frac{\pi^2}{d^2} K\right|} = \frac{\tau_o}{\left|\left(\frac{V}{V_{th}}\right)^2 - 1\right|}. \tag{4.23}$$

Under small angle approximation, the transient phase change is obtained as:

$$\delta(t) \cong \frac{\delta_o}{1 + \left[\frac{\phi_\infty^2}{\phi_o^2} - 1\right]\exp\left(-\frac{2t}{\tau_r}\right)}. \tag{4.24}$$

where δ_o is the total phase change from the voltage-off state to the voltage-on state. By substituting Eq. (4.24) into Eq. (4.8), we obtain the transient transmittance state:

$$I(t) = \sin^2\left(\frac{\delta_o / 2}{1 + \left[\frac{\phi_\infty^2}{\phi_o^2} - 1\right]\exp\left(-\frac{2t}{\tau_r}\right)}\right). \tag{4.25}$$

At $t \to \infty$, the exponential term in Eq. (4.25) vanishes and *I(t)* reaches a plateau:

$$I(\infty) = \sin^2(\frac{\delta_o}{2}). \tag{4.26}$$

To solve the optical rise time, let us assume the transmittance rises from I_1 to I_2 as the time increases from t_1 to t_2. Substituting t_1 and t_2 to Eq. (4.25), we obtain the corresponding transmittance at 10% and 90%:

$$I_1 = 0.1I_o = \sin^2\left(\frac{\delta_o / 2}{1 + \left[\frac{\phi_\infty^2}{\phi_o^2} - 1\right]\exp\left(-\frac{2t_1}{\tau_r}\right)}\right), \tag{4.27}$$

$$I_2 = 0.9I_o = \sin^2\left(\frac{\delta_o / 2}{1 + \left[\frac{\phi_\infty^2}{\phi_o^2} - 1\right]\exp\left(-\frac{2t_2}{\tau_r}\right)}\right). \tag{4.28}$$

By solving t_1 and t_2 from Eqs. (4.27) and (4.28), we derive the optical rise time T_{rise} (10%→90%) as:

$$T_{rise} = t_2 - t_1 = \frac{1}{2}\frac{\tau_o}{\left|\left(\frac{V}{V_{th}}\right)^2 - 1\right|}\ln\left(\frac{\frac{\delta_o/2}{\sin^{-1}\left(\sqrt{0.1}\sin(\frac{\delta_o}{2})\right)} - 1}{\frac{\delta_o/2}{\sin^{-1}\left(\sqrt{0.9}\sin(\frac{\delta_o}{2})\right)} - 1}\right). \quad (4.29)$$

Equation (4.29) correlates the optical rise time (T_{rise}) to the commonly used director rise time (τ_r) as described in Eq. (4.23). Basically, it is a linear relationship except for the additional logarithm term of the phase dependence. As will be discussed in Sec. 4.3, this phase dependence is relatively modest.

4.3 Results and Discussion

To validate Eqs. (4.14) and (4.29), we numerically solve Eq. (4.1) using the finite element method (FEM) [54]. Once the LC director distribution is obtained, we then use the extended Jones matrix method [57], [61] to calculate the transient phase change δ(t).

Figure 11 shows the system configuration of the VA LC under study. A commercial Merck negative nematic MLC-6608 mixture was used in our computer simulations. The material parameters of MLC 6608 are: $n_o = 1.4748$ $n_e = 1.5578$, the dielectric anisotropy $\Delta\varepsilon = -4.2$, the rotational viscosity γ_1 = 186 mPas at 20°C, the splay elastic constant $K_{11} = 16.7\times10^{-12}$ N, twist elastic constant $K_{22} = 7.0\times10^{-12}$ N, and bend elastic constant $K_{33} = 18.1\times10^{-12}$ N. The buffing induced pretilt angle is assumed to be 2° from surface normal unless otherwise mentioned.

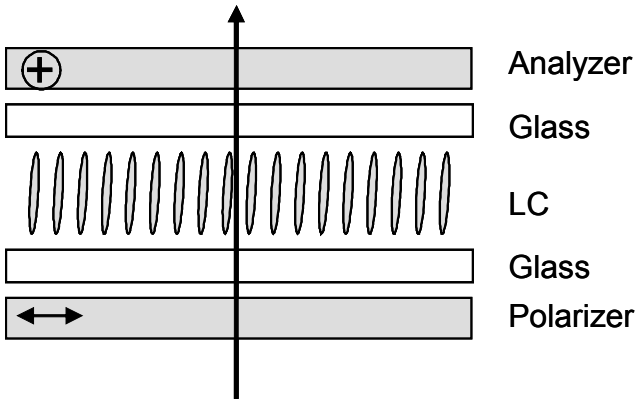

Figure 11: The VA cell used for this study. The LC cell is sandwiched between two crossed polarizers. The inner side of each glass substrate is coated with a thin layer of indium-tin-oxide and polyimide for producing homeotropic alignment. The LC has a small pretilt angle.

For a thin-film-transistor liquid crystal display using transmissive VA cell, the on-state voltage is preferred to be restricted to ~5 V_{rms} for the interest of low power consumption. Therefore, we choose $d\Delta n = 0.7\lambda$, which is slightly larger than the required half-wave phase retardation in order to reduce the on-state voltage. By using MLC-6608, the corresponding cell gap is d =4.64 μm and the total phase retardation is $\delta = 1.4\ \pi$ at λ = 550 nm. Based on Eq. (4.15), the threshold voltage V_{th} is calculated to be 2.19 V_{rms}. At the first transmission peak (i.e., $\delta = \pi$), $V = 2.146\ V_{th}$. We have also studied the response time between gray scales.

4.3.1 Pretilt Angle Effect

For a VA cell, pretilt angle (α) affects the device contrast ratio and response time. Here, we define pretilt angle as the angle of the LC directors deviated from cell normal. If α=0, it implies that the LC directors are aligned perpendicular to the substrate surfaces. Figure 12 plots

the voltage-dependent transmittance (or called VT curve) at α=0.01°, 2°, and 5°. Please note that τ_o was derived by assuming α=0. However, in a real LC device a small pretilt angle is required for LC directors to relax back without creating domains. Therefore, we use α=0.01° to animate the results for α=0. As the pretilt angle deviates from the cell normal, the threshold behavior is gradually smeared and the turn-on voltage is decreased. We have calculated the quantitative LC director reorientation time and optical response time at various voltages for different pretilt angles. However, it will be tedious to tabulate all the results here. To find the tendency while not losing generality, we choose the simulation results with α=0.01° and 2°, as shown in Table 2 and Table 3, respectively.

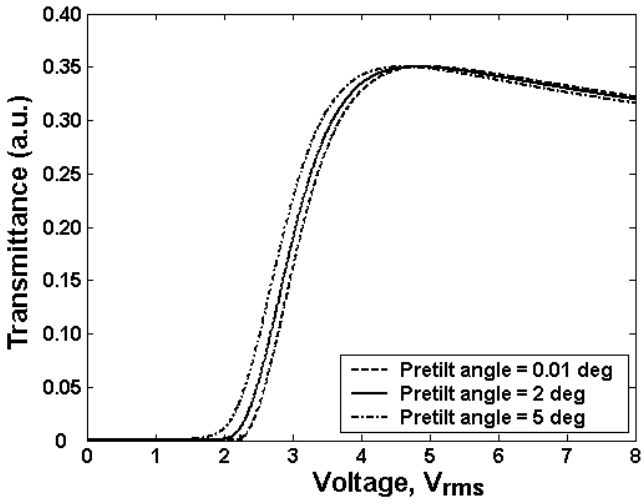

Figure 12: The simulated voltage-dependent transmittance of a VA cell at λ = 550 nm with three different pretilt angles, α = 0.01° (dashed line), 2° (solid line) and 5° (dashed dot line). The parameters used in simulations are listed in the text.

From Table 2, the phase decay time data (the t_p/τ_o column) agree with the LC director decay time quite well in the low voltage regime. Here, to compare with τ_o, we simply calculated the phase decay from 1 to $1/e^2$ (Eq. (4.8)). As the voltage increases, the t_p/τ_o ratio gradually deviates from unity. At V/V_{th} ~1.6, t_p/τ_o increases by ~14%. At $\delta \sim \pi$, the phase decay time is ~23% longer than τ_o. On the other hand, the optical decay time (from 90% to 10%) remains relatively constant (T_{decay}/τ_o~0.65±0.03) in the $V_{th}<V<1.4V_{th}$ regime. As the voltage increases to V/V_{th}~2.15, T_{decay}/τ_o increases to 0.87.

Table 2: Simulation results of phase decay time and optical decay time at different voltages of a VA cell. LC: MLC-6608, d = 4.64 μm, pretilt angle α = 0.01° and V_{th} =2.19 V_{rms}. Here, t_p is the phase decay time, T_{decay} is the optical decay time, and τ_o =22.4 ms is the director's decay time as defined in Eq. (4.5).

Voltage (V_{rms})	V/V_{th}	Phase (π)	t_p (1→1/e^2) (ms)	t_p/τ_o	T_{decay} (90→10%) (ms)	T_{decay}/τ_o
2.30	1.05	0.0640	22.6	1.01	15.1	0.67
2.40	1.10	0.1239	22.8	1.02	14.2	0.63
2.50	1.14	0.1846	23.0	1.03	14.0	0.62
2.60	1.19	0.2452	23.3	1.04	14.0	0.62
2.80	1.28	0.3625	23.7	1.06	14.5	0.65
2.90	1.32	0.4181	24.0	1.07	14.7	0.66
3.00	1.37	0.4709	24.3	1.08	15.1	0.67
3.20	1.46	0.5675	24.8	1.11	15.9	0.71
3.50	1.60	0.6892	25.5	1.14	17.0	0.76
3.70	1.69	0.7558	25.9	1.16	17.7	0.79
4.00	1.83	0.8375	26.5	1.18	18.4	0.82
4.40	2.01	0.9199	27.2	1.21	19.2	0.86
4.70	2.15	0.9672	27.6	1.23	19.5	0.87

Table 3: shows the calculated results for $\alpha = 2°$. A similar trend as that of $\alpha = 0.01°$ is still observed except that both phase and optical decay times are somewhat slower. The theoretical director decay time τ_o is assumed unchanged. The slower phase and optical decay time is believed to originate from the slightly weaker restoring elastic torque due to the increased pretilt angle.

Table 3: Same as Table 2 except the pretilt angle $\alpha = 2°$.

Voltage (V_{rms})	V/V_{th}	Phase (π)	t_p ($1 \rightarrow 1/e^2$) (ms)	t_p/τ_o	T_{decay} ($90 \rightarrow 10\%$) (ms)	T_{decay}/τ_o
2.30	1.05	0.1425	26.4	1.18	16.1	0.72
2.40	1.10	0.1958	26.1	1.17	15.7	0.70
2.50	1.14	0.2516	26.0	1.16	15.5	0.69
2.60	1.19	0.3081	26.0	1.16	15.6	0.70
2.80	1.28	0.4184	26.1	1.17	15.9	0.71
2.90	1.32	0.4706	26.3	1.17	16.3	0.73
3.00	1.37	0.5202	26.4	1.18	16.5	0.74
3.20	1.46	0.6108	26.8	1.20	17.3	0.77
3.50	1.60	0.7246	27.3	1.22	18.4	0.82
3.70	1.69	0.7869	27.7	1.24	19.0	0.85
4.00	1.83	0.8632	28.2	1.26	19.8	0.88
4.40	2.01	0.9404	28.9	1.29	20.3	0.91
4.70	2.15	0.9849	29.3	1.31	20.5	0.92

In Figure 13(a) and (b), we plot the calculated optical decay time ($90\% \rightarrow 10\%$) and rise time ($10 \rightarrow 90\%$), respectively, as a function of V/V_{th} at $\alpha = 1°$, $2°$, $3°$, and $5°$ pretilt angles. The Erickson-Leslie equation was used for these calculations. In general, at a given V/V_{th} a smaller pretilt angle would lead to a faster decay time but slower rise time. In the vicinity of threshold, the rise time is particularly slow, as described in Eq. (4.23). As the voltage increases, the optical

rise time is decreased rapidly. At $V \sim 2.2V_{th}$ (peak transmittance), the rise time is reduced to ~10 ms.

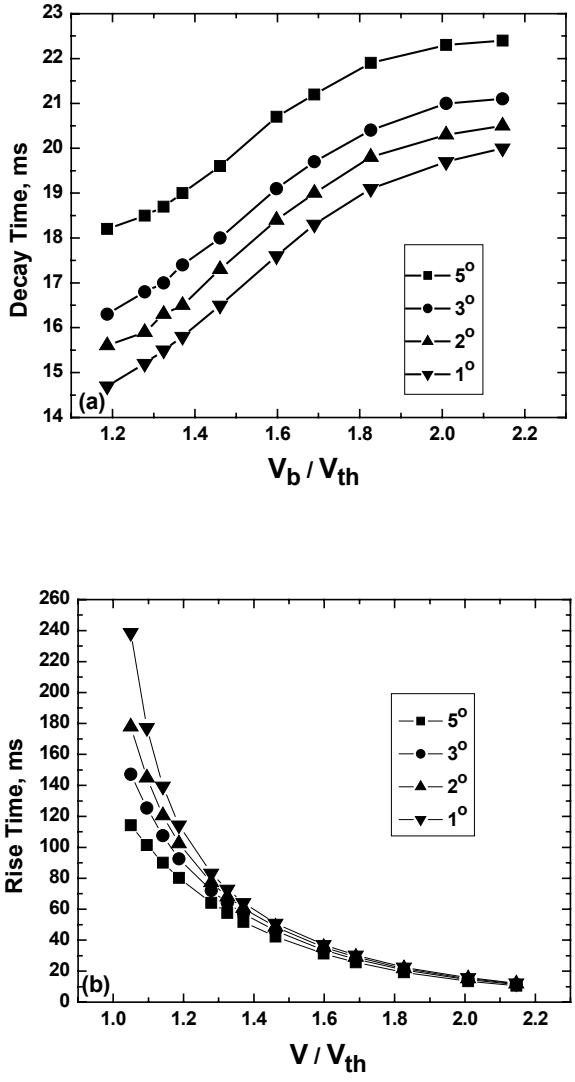

Figure 13: (a) Optical decay time (90%→10%) and (b) rise time (10%→90%) as a function of V/V_{th} at four different pretilt angles, α = 1°, 2°, 3°, and 5°.

Strictly speaking, the threshold behavior exists only when the pretilt angle is zero. However, in most LC devices a non-zero pretilt angle is required in order to avoid domain formation during molecular reorientation. The free relaxation time τ_o is derived based on the assumptions that α=0 and the applied voltage is not too far above the threshold. In reality, these assumptions may not be valid. Taking into account the pretilt angle effect, we modify the free relax time according to the following equation:

$$\tau_o^* = \beta\tau_o, \tag{4.30}$$

where τ_o is the free relaxation time when pretilt angle is zero, and can be calculated according to Eq. (4.5). In Eq. (4.23), τ_o is dependent on the pretilt angle. Since most of display cells have a pretilt angle, this correction factor is necessary to match theory with experimental results [84]. We have used the Erickson-Leslie equation to calculate the LC response time including pretilt angle effect but without using the small angle approximation. The β values we found are listed in Table 4. At a very small pretilt angle α ~0.01°, $\tau_o^* \sim \tau_o$; i.e., the correction factor β=1, as expected. As the pretilt angle increases, β gradually increases. At α=5°, β is found to be higher than the ideal value, which is unity, by nearly 30%.

The pretilt angle is dependent on the polyimide alignment layer, rubbing strength, and LC material employed [85], [86]. For a given polyimide alignment layer, different LC materials may have a slightly different pretilt angle depending on the molecular interactions. The typical pretilt angle for a VA cell is ~2°. Thus, β ~1.16 has been taking into consideration whenever we calculated the response time of a VA cell with α=2°.

Table 4: Pretilt angle effect on the LC director's decay time τ_o^*.

Pretilt angle α(°)	τ_o^* / τ_o
0.01	1
1	1.10
2	1.16
3	1.21
5	1.30

4.3.2 Gray Scale Switching

The beauty of a nematic LCD is that it has natural gray scales. Each primary color (red, green, and blue) can display 8-bits gray scales. Thus, a full-color display with 16 million colors can be obtained. To investigate gray scale switching, we divide the voltage-dependent transmittance curve into eight equal intensity gray levels, as shown in Figure 14. Level 1 represents the dark state and level 8 for the brightest state. The maximum transmission shown in Figure 14 is 35% after taking the absorption of the polarizer and analyzer into consideration.

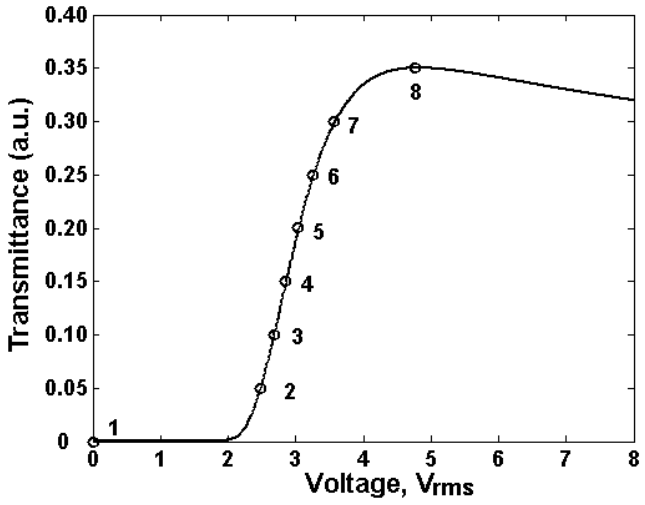

Figure 14: The eight gray levels of the VA cell at λ = 550 nm LC: MLC-6608, d = 4.64 μm and pretilt angle α = 2°.

Table 5 lists the calculated optical response time using the finite element and finite difference time domain methods for both decay and rise processes of the eight-level gray scales. The data in the right top triangle represent the rise time, while the left bottom are the decay time. The rise time from gray level 1 to 2 is the slowest because the applied voltage is so close to the threshold voltage. In a VA cell, gray scale 1→2 represents the switching from the darkest state to the second darkest state. Although it is slow, it is forgiven because human eye could not resolve this change too well. In the high voltage regime, gray scale switching is relatively fast. The actual switching time depends on the cell gap and visco-elastic coefficient (γ_1 / K_{33}) of the LC material employed. To improve the switching speed between gray levels, the over-drive and undershoot method has been proposed and implemented in real display devices [3], [4]. The data in the first row and the first column will be further used in our correlation.

Table 5: The calculated eight gray level optical rise time (10%→90%) and decay time (90%→10%) of the VA cell shown in Figure 14.

Decay time, ms \ Rise time, ms	**1**	**2**	**3**	**4**	**5**	**6**	**7**	**8**
1		124.5	90.7	72.1	58	45.7	33.1	11.3
2	15.5		69.4	58.9	49.2	39.8	29.2	9.6
3	15.7	70.8		53.6	45.5	37.1	27.5	8.6
4	16.1	64.4	57.5		43.4	35.7	26.6	8
5	16.7	60.2	54.7	48.5		34.9	26.2	7.4
6	17.5	57.4	52.9	47.4	41.3		26.2	7.0
7	18.6	55.8	52.1	47.1	41.6	35.2		6.4
8	20.5	55.9	53	48.7	43.8	38.3	31.3	

4.3.3 Detailed Correlations

In this section, we show the detailed simulation results between the director reorientation time and optical response time. The Erickson-Leslie equation was used for these calculations. A good correlation between the LC director reorientation time and optical response time is found.

4.3.3.1 Decay Time

In the small angle approximation, one of the important assumptions is $\sin(\theta) \sim \theta$. Under such a circumstance, the analytical form of LC director reorientation time constant τ_o can be derived. However, the LC director reorientation time is difficult to measure directly in an experiment. For display applications, the optical response time is a more practical term. How to correlate the LC director reorientation time to the measurable optical response time is an important task.

Figure 15(a) depicts the director distribution ($\phi(z)$) as a function of normalized cell gap (z/d) at $V \sim 1.37\ V_{th}$. Although the voltage is not too high from threshold, a large director deformation has already occurred. In the middle layer, the maximum director tilt angle (ϕ_m) has reached ~53°. Therefore, it is difficult to foresee whether the small angle approximation still holds. If it does, then Eq. (4.8) should be valid and $\ln[\delta_o / \delta(t)]$ should be a linear function of time with slope equal to $2/\tau_o$. From the slope measurement, τ_o can be extracted.

In experiment, the VA cell sandwiched between crossed polarizers is biased at a voltage V_b. When the LC cell relaxes from V_b to 0, the total phase change is δ_o. For a VA cell intended for intensity modulation, $\delta_o \le \pi$. When the voltage is released instantaneously at t =0, the time-

dependent transmittance is recorded. This time-dependent transmittance can be converted to the transient phase decay described by $\delta(t)$. Figure 15(b) plots the calculated $\ln[\delta_o / \delta(t)]$ as a function of time for the VA cell. Indeed, a straight line with slope of 0.0755/ms is obtained. Based on this slope, $\tau_o = 26.5$ ms is found. Using the LC parameters, we find $\tau_o = 22.4$ ms from Eq. (4.5) and $\tau_o^* = 26$ ms from Eq. (4.28) with β =1.16 because of the 2° pretilt angle. The agreement between the small angle approximation and the Erickson-Leslie equation is amazingly good in this case.

Next, we validate the correlation between the optical decay time (T_{decay}) and the director's decay time (τ_o), as expressed in Eq. (4.14). If we neglect the logarithm term, then T_{decay} =0.5 τ_o; the observed optical response time is 2X shorter than that of the LC director decay time. With the phase-dependent term included, the change is still not too significant. Figure 16 plots T_{decay}/τ_o at different δ_o, as described in Eq. (4.14). In Figure 16, circles represent the simulation results using the Erickson-Leslie equation, while the solid line represents the small angle approximation. In the small δ_o region, i.e., V is not too far above V_{th}, the agreement between these two methods is reasonably good. As δ_o increases, the discrepancy increases slightly. At the biased voltage V_b/V_{th} =2.146 which corresponds to $\delta_o \sim 1\pi$, the maximum error observed is ~14 %.

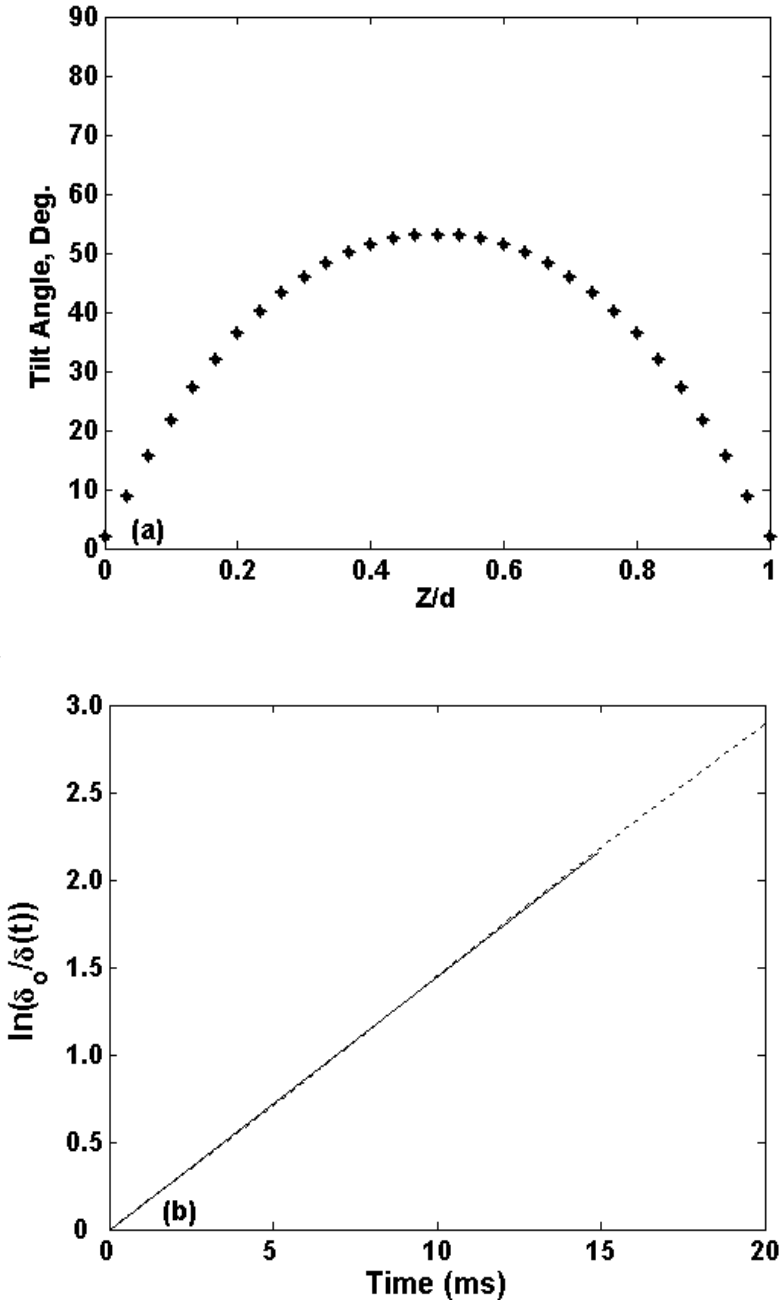

Figure 15: (a) The calculated LC director distribution $\phi(z)$ as a function of normalized cell gap (z/d). (b) Time-dependent $\ln[\delta_o / \delta(t)]$ of the VA cell. Dots are calculated data and solid line is the fitting curve. From the slope of the straight line, τ_o^* is found to be ~26 ms.

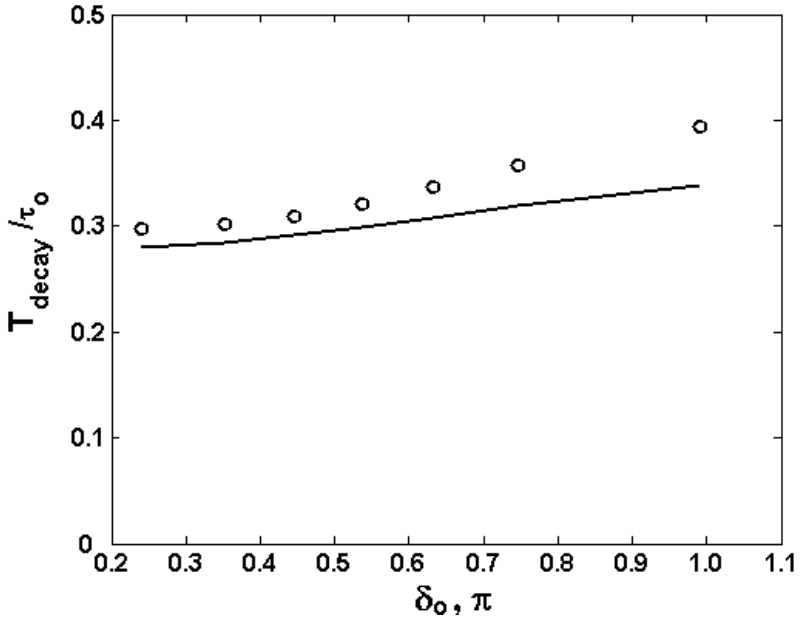

Figure 16: The correlation of the optical decay time T_{decay} (90%→10%) vs. the LC director reorientation time (τ_o) as a function of δ_o. Circles represent the simulation results using the Erickson-Leslie equation, while the solid line is the correlation obtained from the small angle approximation [Eq. (4.14)].

4.3.3.2 Rise Time

Rise time is much more difficult to solve than the decay time because it also depends on the applied voltage. Equation (4.29) correlates the optical rise time with the LC director rise time. At a given voltage, the optical rise time is 2X shorter than the LC director rise time if we neglect the logarithm term. Even the phase dependence term is included, the results are not affected too greatly. Figure 17 depicts the ratio of T_{rise}/τ_o at different δ_o as described by Eq. (4.29). In Figure 17, circles represent the simulation results using the Erickson-Leslie equation,

while the solid line represents the small angle approximation. A very good agreement is obtained except in the near threshold region.

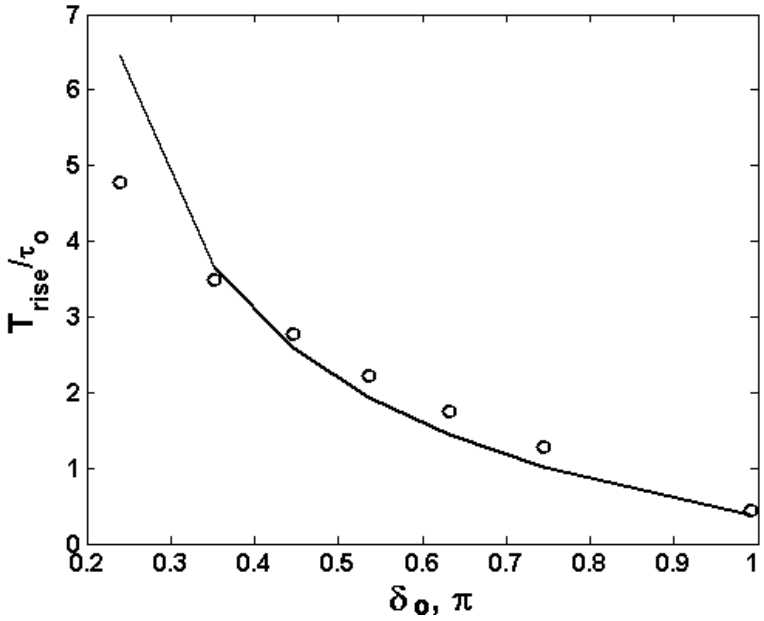

Figure 17: The correlation of optical rise time T_{rise} (10%→90%) vs. the director reorientation time (τ_o) as a function δ_o. Circles represent the simulation results using the Erickson-Leslie equation, while the solid line is the correlation obtained from the small angle approximation [Eq. (4.29)].

When V_b gets close to V_{th}, the pretilt angle effect becomes more pronounced. In our simulations, pretilt angle is assumed to be 2°. Due to the smeared and decreased threshold, the required voltage for obtaining $\delta_o \sim 0.25\pi$ is lower. As a result, the calculated rise time is longer than τ_o, as indicated by Eq. (4.23).

4.4 Conclusion

We have derived the correlations between the LC director reorientation time and the optical response (both decay and rise) time of a vertically aligned cell. Results indicate that the optical response time (T_{rise} and T_{decay}) is linearly proportional to the LC director reorientation time. The initial bias voltage effect is not too strong. Pretilt angle is found to make an important impact to the LC dynamics. To correct for the pretilt angle effect, a modified rotational viscosity needs to be used.

CHAPTER 5: BACKFLOW EFFECT ON THE DYNAMIC RESPONSE OF LIQUID CRYSTAL PHASE MODULATOR

5.1 Introduction

Liquid crystal (LC) optical phased array (OPA) [36] is an efficient device for laser beam steering. In an OPA, a blazed phase grating is generated by controlling the spatial voltage patterns of the pixilated electrodes. The incoming linearly polarized light interacts with the phase grating and gets deflected. The steering angle (or the deflection angle) can be as large as 5-7^o depending on the electrode gap and birefringence of the LC employed. For achieving a pure phase modulation, nematic LC with homogeneous alignment is commonly used. In a homogeneous cell, the maximum obtainable phase difference due to the voltage-induced molecular reorientation is $\delta = 2\pi d\Delta n / \lambda$, where d is the cell gap, Δn is the birefringence, and λ is the wavelength. For laser beam steering at λ =1.55 μm, the required 2π phase change leads to $d\Delta n$~1.55 for a transmissive OPA. This dΔn requirement is ~3X higher than that of a visible wavelength. Moreover, due to the birefringence dispersion effect [87] the LC birefringence drops ~20% in the near IR region as compared to that at λ =550 nm. For the interest of achieving a fast response time, using a thin LC cell with a high birefringence LC is a favorable approach. Due to the thin cell gap, a relatively high (10 V_{rms}) voltage is needed in order to completely reorient the LC directors. Under such a driving condition, backflow is inevitable in the dynamic response [88],[89].

The response time of a homogeneous LC cell is proportional to $\gamma_1 d^2 / \pi^2 K_{11}$, where γ_1 is the rotational viscosity and K_{11} is the splay elastic constant [72]. To achieve a fast response

time, high birefringence and low viscosity materials are particularly desirable [1],[2]. High birefringence enables a thinner cell gap to be used so that the response time is faster. Low viscosity is also helpful for reducing the response time. A simple method for reducing viscosity is to operate the LC device at an elevated temperature. As the temperature increases by 10 °C, the viscosity decreases by ~2X.

The available data on the viscous properties of LC materials are almost always incomplete. So far, the only complete set of the six Leslie viscosity coefficients [78] was published by Kneppe and Schneider about two decades ago in their complicated rotating magnetic field experiments [90]. The LC compound studied was 4-methoxybenzylidene-4'n-butylaniline (MBBA). However, MBBA is not a practical compound for OPA applications because of its poor material stability. Presently, many commercial high birefringence LC mixtures are based on cyano-biphenyl and -terphenyl compounds. To study the dynamical response of OPA, it is necessary to find an effective method to estimate the Leslie coefficients for high birefringence LC mixtures.

In our experiments, we used E7 LC mixture (Merck) and a high birefringence and low viscosity LC mixture, UCF-2 [1],[2], as exemplary materials for validating our model. In Sec. 5.2, we derive the dynamic response of LC including backflow at various temperatures. In Sec. 5.3, we briefly describe the experimental methods. In Sec. 5.4, we extend the temperature-dependent Leslie viscosity coefficients of MBBA to E7 based on the Imura and Okano (IO) theory [91]. We first justify the α_2 and α_4 of E7 using the experimental data and then validate the fitting equations by the experimental data. Using these parameters, we simulate the OPA dynamics including backflow effect. The agreement between theory and experiment is excellent.

5.2 Theoretical Background

5.2.1 Erickson-Leslie Equation

In the dynamic Freedericksz transition of a homogeneous nematic cell, the azimuthal angle ϕ is constant so that the LC director can be solely described by the tilt angle $\theta(z,t)$. The motion of the LC director is coupled with the flow ν in the x direction. The evolution of θ and ν under an applied voltage is governed by the following Erickson-Leslie equation [78],[79], which takes into account the balance of elastic and electric-field-induced torques:

$$I\frac{\partial^2\theta}{\partial t^2}+\gamma_1\frac{\partial\theta}{\partial t}=\left(K_{11}\cos^2\theta+K_{33}\sin^2\theta\right)\frac{\partial^2\theta}{\partial z^2}+(K_{33}-K_{11})\sin\theta\cos\theta\left(\frac{\partial\theta}{\partial z}\right)^2 + \varepsilon_o\Delta\varepsilon E^2\sin\theta\cos\theta+(\alpha_2\sin^2\theta-\alpha_3\cos^2\theta)\frac{\partial v}{\partial z}, \tag{5.1}$$

where α_i are the Leslie viscosity coefficients, I is the inertia of the LC, θ is the polar angle of the LC director (the angle between the LC director and the x-y plane, as depicted in Figure 18), K_{ii} are the Frank elastic constants, $\Delta\varepsilon$ is the dielectric anisotropy, and v is the flow velocity.

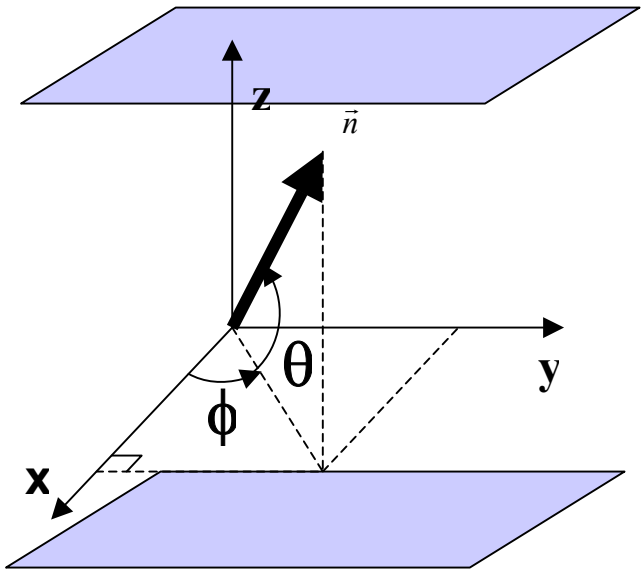

Figure 18: The coordinate system of LC director, where θ is the tilt angle of the LC director, which is the angle between the LC director and the x-y plane, and ϕ is the angle between projection of the LC director on the x-y plane and the x-axis.

In general, the inertial effect is much smaller than the elastic and viscous torques and can be neglected. Neglecting the inertial term, the flow velocity is governed by:

$$\frac{\partial}{\partial z}\left\{\left(\alpha_3\cos^2\theta-\alpha_2\sin^2\theta\right)\frac{\partial\theta}{\partial t}+\frac{1}{2}\left[2\alpha_1\sin^2\theta\cos^2\theta+(\alpha_5-\alpha_2)\sin^2\theta+(\alpha_3+\alpha_6)\cos^2\theta+\alpha_4\right]\frac{\partial v}{\partial z}\right\}=0. \tag{5.2}$$

Solving $\partial v/\partial z$ from Eq. (5.2), and substituting this into Eq. (5.1), we obtain the effective rotational viscosity γ_1^* as [92]:

$$\gamma_1^*=\gamma_1-\frac{(\alpha_2\sin^2\theta-\alpha_3\cos^2\theta)^2}{\frac{1}{2}[2\alpha_1\sin^2\theta\cos^2\theta+(\alpha_5-\alpha_2)\sin^2\theta+(\alpha_3+\alpha_6)\cos^2\theta+\alpha_4]}, \tag{5.3}$$

where γ_1 is the rotational viscosity, and $\alpha_i's$ are the Leslie coefficients. In the low voltage regime ($V < V_{th}$) of a homogeneous (splay-mode) cell, γ_1^* can be approximated by γ_s^*, where [92]:

$$\gamma_s^*=\gamma_1^*(\theta=0)=\gamma_1-\frac{2\alpha_3^2}{\alpha_3+\alpha_6+\alpha_4}=\gamma_1-\frac{2\alpha_3^2}{2\alpha_3+\alpha_2+\alpha_5+\alpha_4}. \tag{5.4}$$

At a higher offset voltage ($V >> V_{th}$), the LC directors are reoriented perpendicular to the substrates except the boundary layers. Thus, the effective rotational viscosity (γ_B^*) for the bend-mode ($\theta = 90°$) is [92]:

$$\gamma_B^*=\gamma_1^*(\theta=90)=\gamma_1-\frac{2\alpha_2^2}{-\alpha_2+\alpha_4+\alpha_5}. \tag{5.5}$$

It is evident from Eqs. (5.4) and (5.5) that in a splay or bend mode, the director reorientation depends largely on α_2 and $\alpha_4 + \alpha_5$; the α_3 values are one to two orders of magnitude smaller and are neglected. Similar effect is also observed in the twisted nematic cell [93]. For laser beam steering, we need a pure phase modulator with phase change $\delta \geq 2\pi$. The pure phase modulation of a TN cell has been demonstrated in the low voltage regime; below the optical Freederisckz transition threshold [94]. However, to archive the required 2π phase change, the TN cell gap would be too large so that the response time would be too slow. Both homogeneous and homeotropic cells can be used for pure phase modulation. However, from a molecular design standpoint it is easier to obtain LC compounds with a large and positive $\Delta\varepsilon$. Thus, here we focus on the LC directors' deformation of a homogeneous cell with strong anchoring at surface boundaries.

5.2.2 Temperature Effect

Temperature has a great influence on the physical properties of a thermotropic LC. As temperature increases, the birefringence, dielectric anisotropy, viscosity, and elastic constant all decrease but at different rates. The temperature-dependent physical properties are governed by the order parameter S as [95]:

$$\Delta n = (\Delta n)_o S, \tag{5.6}$$

$$\Delta\varepsilon = A\frac{S}{T}, \tag{5.7}$$

$$K_{ii} = (K_{ii})_o S^2, \tag{5.8}$$

$$\gamma_1 = bS\exp(E'/k_0 T), \tag{5.9}$$

where $(\Delta n)_o$ and $(K_{ii})_o$ are the birefringence and elastic constant, respectively, at S=1, i.e., T=0 K, A and b are proportionality constants, E' is the activation energy of molecular rotation, and k_0 is the Boltzmann constant. If the temperature is not too close to T_c, the order parameter S can be approximated as [80]:

$$S = (1 - T / T_c)^{\beta}. \tag{5.10}$$

Equation (5.10) is Haller's approximation for the order parameter where T_c is the clearing point of the LC mixture and β is a material constant. The ratio of $T_r = T / T_c$ is called reduced temperature. This approximation holds quite well if the temperature is not too close to the clearing temperature. The exponent β is dependent on molecular structure, but not on wavelength. For most LC compounds studied, $\beta \approx 0.20$. For the E7 LC mixture we studied, T_c =333 K. From the measured temperature-dependent birefringence data, we obtain $(\Delta n)_o$=0.304 and $\beta = 0.222$. These results are consistent with the published literature values [40].

5.2.3 Temperature-dependent Leslie Coefficients

In the Imura and Okano theory, all six Leslie coefficients (α_1-α_6) are expressed in terms of the order parameter S as [95]:

$$\alpha_1 = A_1 S^2, \tag{5.11}$$

$$\alpha_2 = -(B_1 + C_1)S - (B_2 + C_2)S^2, \tag{5.12}$$

$$\alpha_3 = -(B_1 - C_1)S - (B_2 - C_2)S^2, \tag{5.13}$$

$$\alpha_4 = 2\eta_{is} - aS + A_3 S^2, \tag{5.14}$$

$$\alpha_5 = (\frac{3}{2}a + B_1)S + (A_2 + B_2)S^2, \tag{5.15}$$

$$\alpha_6 = (\frac{3}{2}a - B_1)S + (A_2 - B_2)S^2, \tag{5.16}$$

where the coefficients a, A_i, B_i and C_i (i =1, 2) are weakly dependent on the temperature. For different LC materials, for simplicity let use assume that these coefficients (a, A_i, B_i and C_i) remain unchanged but the order parameter would vary due to different β and T_c.

According to the definitions, $\gamma_1 = \alpha_3 - \alpha_2$ and $\gamma_2 = \alpha_6 - \alpha_5$. Based on the Parodi relationship [97], γ_2 can be rewritten as $\alpha_3 + \alpha_2$. In Eq. (5.14), η_{is} is the flow viscosity of the LC in the isotropic state

$$\eta_{is} = \eta_o \exp(E / k_B T), \tag{5.17}$$

where E >0 is the activation energy of molecular diffusion, and η_o is a proportionality constant. Equation (5.17) is the well-known Arrhenius law for isotropic liquids.

5.2.4 Method to Estimate Leslie Coefficients

Based on the above discussion, we propose a method to estimate the Leslie coefficients. So far, the only complete set of Leslie coefficients was published for MBBA using the rotating magnetic field experiments [90]. Using the MBBA data to fit Eqs. (5.11)–(5.17), we found E= 0.414 eV. During fittings, we have assumed that all the coefficients a, A_i, B_i and C_i (i =1, 2) are constants and used the recommended six Leslie coefficients of MBBA listed in Table 6.

Using the MBBA data to fit the IO theory, we obtain a set of coefficients, listed in Table 7. From these fittings, we find that the experimental data fit reasonably well with the IO theory

for α_4, α_5, and α_6, but poorly for α_1, α_2, and α_3. For α_1, a better fitting is found if we include a third-order S term in Eq. (5.11):

$$\alpha_1 = (A_4 S + A_5) S^2, \tag{5.18}$$

where A_4 = 0.2072 Pa s and A_5 = 0.0748 Pa s. The fitting result of α_1 in Eq. (5.18) is sketched in Figure 19 (a), where open circles represent the measured results and filled circles are the fitting results. The agreement between fitting and experiment is very good. Also included in Figure 19 (b) for comparison are the fitting results using Eq. (5.11). Without the third order term, the fitting of Eq. (5.11) with experiment is quite unsatisfactory.

Table 6: Recommended Leslie coefficients for MBBA (from Ref [90]). All α_i's are in unit of Pa s. S is calculated from $S = (1 - T/T_c)^{\beta}$ with β = 0.188 and T_c = 319.2 K.

T (C)	S	α_1	α_2	α_3	α_4	α_5	α_6
20	0.625	-0.0215	-0.1534	-.00077	0.1095	0.1071	-0.0471
25	0.600	-0.0181	-0.1104	-.00110	0.0826	0.0779	-0.0336
30	0.571	-0.0141	-0.0800	-.00151	0.0644	0.0572	-0.0244
35	0.533	-0.0095	-0.0573	-.00194	0.0515	0.0417	-0.0176
40	0.477	-0.0054	-0.0387	-.00223	0.0422	0.0285	-0.0124
42	0.443	-0.0036	-0.0310	-.00218	0.0394	0.0224	-0.0109
44	0.392	-0.0012	-0.0210	-.00179	0.0374	0.0136	-0.0092

Table 7: Parameters obtained from fitting MBBA data with the IO theory (Eqs. (5.11)–(5.17)). All the parameters are in units of Pa s.

A_1	B_1	C_1	B_2	C_2	η_o	a	A_2	A_3
-0.0417	-0.1442	-0.1568	0.4004	0.4179	4.33×10^{-9}	-0.0437	0.1729	-0.0829

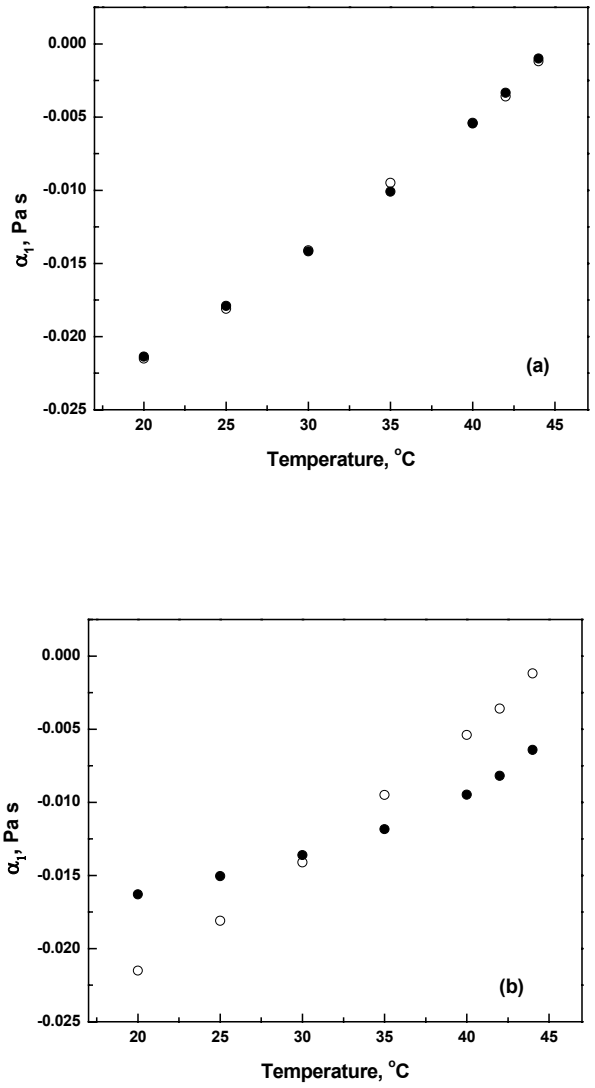

Figure 19: The Fitting results of α_1 for MBBA (a) using Eq. (5.18) and (b) using Eq. (5.11). Open dots are measured data and filled dots are the fitting results.

The rotational viscosity is related to the Leslie coefficients (α_3 and α_2) as $\gamma_1 = \alpha_3 - \alpha_2$. From Eqs. (5.12) and (5.13), we obtain the following expression for γ_1:

$$\gamma_1 = 2C_1 S + 2C_2 S^2. \tag{5.19}$$

However, Eq. (5.19) does not fit the MBBA data well, as shown in Figure 20. A better fitting is found using the following expression proposed by Wu and Wu [98]:

$$\gamma_1 = bS \exp(E' / k_0 T). \tag{5.20}$$

In Eq. (5.20), b is the proportionality constant, E' is the activation energy of molecular rotation, and k_0 is the Boltzmann constant. From Eq. (5.20), the activation energy E', which is determined by the LC structures, has a dramatic effect on the rotational viscosity.

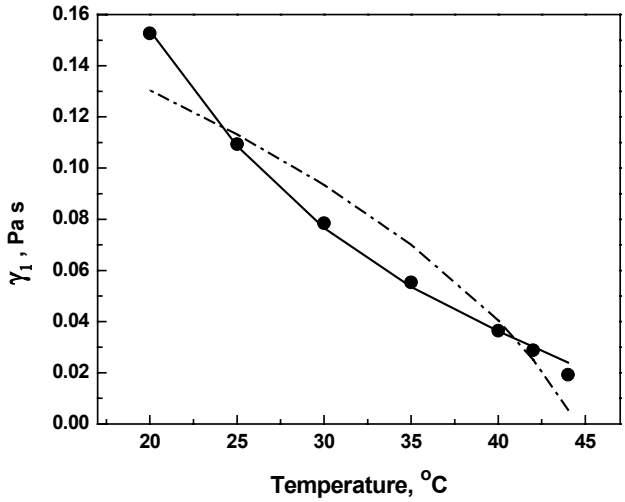

Figure 20: The temperature-dependent rotational viscosity of MBBA. Dots are the experimental data calculated from Table 6, dashed lines are fitting results using Eq. (5.19), and solid line is fitting using Eq. (5.20).

Figure 20 plots the MBBA data (dots) and fitting results using Eq. (5.19) (dashed lines) and Eq. (5.20) (solid line). It is obvious that Eq. (5.20) has a much better fitting than Eq. (5.19). From Table 6, the α_3 of MBBA is negative but very close to zero, which leads to:

$$\alpha_2 \approx -\gamma_1 = -bS\exp(E'/kT). \tag{5.21}$$

Thus, α_2 can be determined through the measurement of γ_1. Therefore, in our simulations we use Eqs. (5.18) and (5.21) for α_1 and α_2, and Eqs. (5.14)-(5.16) for α_4, α_5 and α_6, respectively. In the following, we will validate this method by comparing the experimental and simulation results using two LC mixtures, E7 and UCF-2.

5.3 Experiment

In experiments, we measured the physical properties such as birefringence and visco-elastic coefficient of E7 and UCF-2 using homogeneous cells. The inner sides of the indium-tin-oxide glass substrates were coated with a thin polyimide layer and then rubbed in anti-parallel directions. The buffing induced pretilt angle is ~3° and the anchoring energy is ~3×10^{-4} J/m^2 [101]. The cell gap was determined from the transmitted interference fringes through a spectrophotometer. The cell gap was found to be d =13.4μm for E7 and 7.81 μm for UCF-2. The elastic and dielectric constants of E7 and UCF-2 were measured using a computer-controlled APT III manufactured by Displaytech. The birefringence (Δn) was determined by measuring the voltage-dependent transmittance of the LC cell at λ =1.55μm through the LabVIEW data acquisition system [99]. Table 8 lists the measured physical properties of E7 at T =20.3, 33.3, and 46.9 °C.

For the temperature studies, the cell was held in an oven (INSTEC STC-200D) which has 0.2 °C stability. To mimic the operating condition of an OPA, the LC cell was initially biased at V_i =10 V_{rms}. During the relaxation process, the voltage was removed at t=0 and the optical response monitored by the photodiode detector and displayed by a digital oscilloscope.

Table 8: Some measured and calculated LC parameters of E7 at various temperatures. λ =1.55 μm and T_c =60°C.

T (°C)	K_{11} (pN)	K_{33} (pN)	$\varepsilon_{//}$	$\Delta\varepsilon$	Δn	α_1 (mPa·s)	α_2 (mPa·s)	α_3 (mPa·s)	α_4 (mPa·s)	α_5 (mPa·s)	α_6 (mPa·s)
20.3	11.7	19.5	19.6	14.5	.190	-21.2	-281.8	-1.0	224.7	92.1	-190.6
33.3	10	16.5	17	12	.175	-14.2	-123.5	-1.4	120.4	67.2	-57.7
46.9	7	10	15	10	.148	-6.2	-52	-1.9	70	34	-19.9

5.4 Results and Discussion

To compare with the experimental results, we numerically solved Eq.(5.1) using the finite element [83] and finite difference time domain methods assuming that the anchoring energy is infinite. The dynamic response of two LC mixtures was studied: E7 and UCF-2. E7 was used in the first generation OPA. However, its figure of merit [100], defined as $FoM = K_{11}(\Delta n)^2 / \gamma_1$, is only ~4 ms/μm^2 at T ~48°C. To enhance FoM, we formulated a new mixture (UCF-2) consisting of isothiocyanato-tolane compounds. The FoM of UCF-2 reaches ~40 ms/μm^2 at T =70°C. As a result, the OPA would have a much faster response time. However, the backflow effect needs to be investigated.

5.4.1 E7

Figure 21 depicts the voltage-dependent transmittance curves at λ =1.55 μm and three different temperatures, T = 20.3°C (gray line), 33.3°C (dot-dashed line), and 46.9°C (solid line). From these curves, we find that the birefringence of E7 at λ =1.55 μm is Δn =0.190, 0.175, and 0.148 at T =20.3, 33.3, and 46.9 °C, respectively.

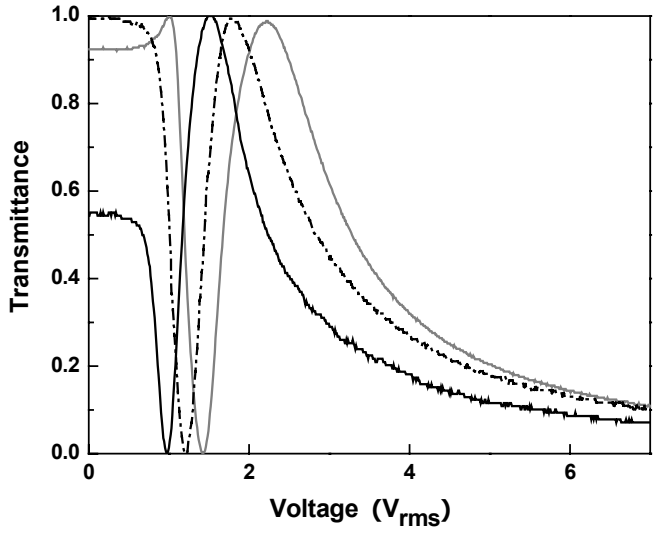

Figure 21: Voltage-dependent transmission of a 13.4-μm-thick homogeneous E7 cell between crossed polarizers at three different temperatures: T =20.3°C (gray line), 33.3°C (dot-dashed line) and 46.9°C (solid line). λ =1.55 μm.

The temperature-dependent rotational viscosity of E7 is shown in Figure 22 where the dots are the measured data and the solid line represents the fitting curve using Eq. (5.20). To fit the experimental data, we use the same β (=0.222) for the order parameter (S) and a, {Ai, Bi, Ci} (i=1, 2), and A3, A4, and A5 as MBBA and leave b and E' as adjustable parameters. From the fittings, we find b=1.3x10^{-8} Pa s and E' = 0.439eV for E7. The obtained activation energy agrees

very well with that reported in [81] (E' =0.440 eV). The relatively large E' is caused by the dimmer formation of cyano-biphenyls in the E7 mixture.

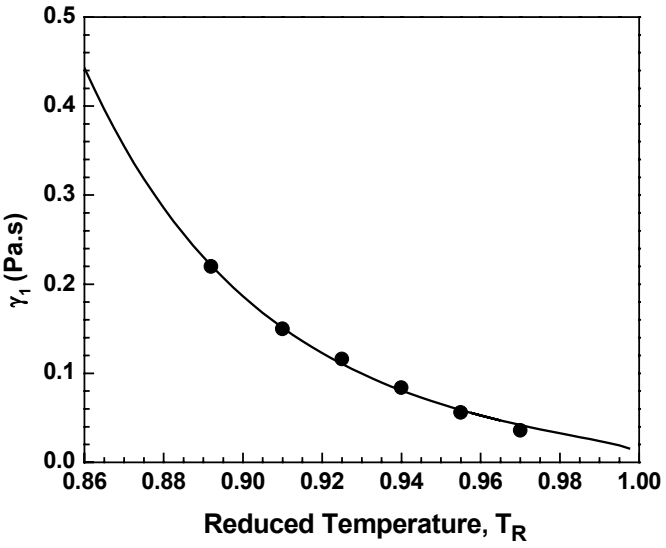

Figure 22: The temperature dependent γ_1 of E7. Dots are measured data and solid lines are the fitting curves using Eq. (5.20).

Figure 23 plots the measured optical dynamic response of the E7 LC cell at T= 20.3°C (grey line), 33.3°C (dashed line), and 46.9°C (solid line), respectively. Before relaxation starts, the LC cell was biased at V_b =10 V_{rms}. Under such a circumstance, the LC directors are reoriented almost perpendicularly to the substrates throughout the bulk except the boundary layers. These boundary layers still preserve some residual phase retardation. Thus, under crossed-polarizer conditions, a small transmittance is observed at t =0, as shown in Figure 23. This residual transmittance is affected by the dΔn, threshold voltage, and surface anchoring energy of the LC cell. As the temperature increases, both birefringence and threshold voltage decrease. Thus, the initial transmittance is suppressed. Moreover, the rotational viscosity

decreases as the temperature increases. Thus, the time required to reach the first transmittance peak is reduced.

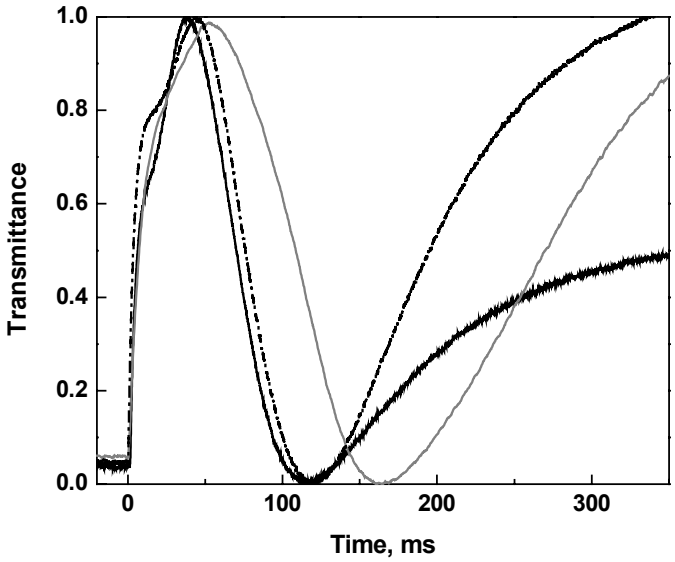

Figure 23: The experimental optical dynamic responses of a homogeneous E7 cell at three different temperatures: T = 20.3°C (grey line), 33.3°C (dot-dashed line) and 46.9°C (solid line). d =13.4 μm and λ = 1.55 μm.

In Figure 23, the backflow effect is clearly observed in the first few milliseconds. At the first stage of relaxation, the transmittance curve shows a steeper slope at each temperature due to the backflow effect. During the abrupt relaxation, the LC directors initially overshoot with time and attain a maximum value at a very short time before decaying monotonically to zero. Figure 24 shows the simulated tilt angle distributions of the E7 cell at T = 46.9°C during its first 30 ms relaxation. At t =0, the 10 V_{rms} biased voltage is removed instantaneously. Right before the electric field is removed, the bulk molecules are reoriented to be perpendicular to the substrates

except the boundary layers due to their pretilt angle and strong surface anchoring. The tilt angle increases to beyond 90° with time so that the LC molecules are driven to the opposite direction. At t ~10 ms, the tilt angle reaches its maximum value. Afterwards, the tilt angle starts to decay and the molecules are driven back to the forward direction. This flow-induced phenomenon occurs normally when the strength of the field is well above the threshold and the field transition is abrupt. At the center of the cell, there exists equal but 'opposite' torques, so the molecules are driven to the opposite direction temporarily. After the initial backflow, the velocity decreases quickly, changes sign, and finally approaches zero. Van Doorn [88] and Berreman [89] have numerically analyzed the director reorientation independently.

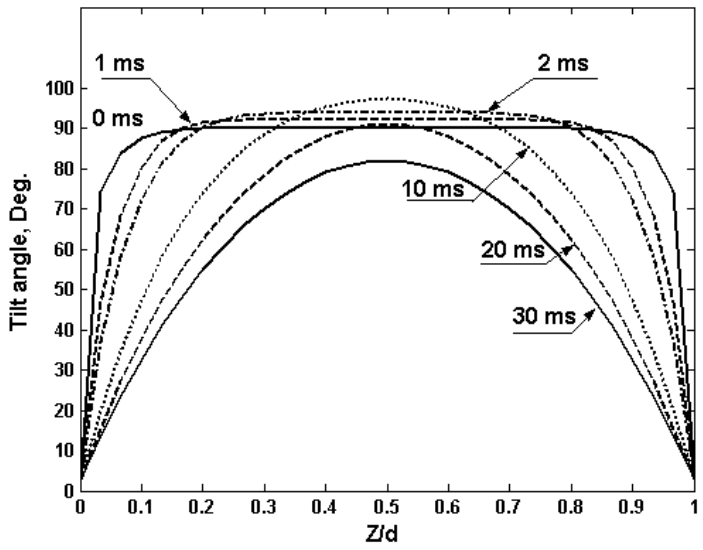

Figure 24: The simulated tilt angle distribution of a homogeneous E7 cell at T = 46.9°C during its first 30 ms relaxation. d =13.4 μm and λ =1.55 μm. The parameters used for simulations are listed in Table 8.

The transient optical dynamic response of the E7 cell at three different temperatures, T = 20.3, 33.3, and 46.9 °C are shown in Figure 25 (a-c), respectively. In these figures, the solid lines represent the experimental results and the dashed lines show the simulation results. The parameters used for the simulations are listed in Table 8. The general agreement between the simulations and experimental results is quite good. As already discussed in theory, the director reorientation depends largely on α_2 and $\alpha_4+\alpha_5$ in the form of Eq. (5.4). In our simulations, we only adjusted the α_4 value to best fit the experimental results at each temperature. The values of α_4 in Table 8 have already been updated for the best fittings. Here, we need to mention that the choice of α_4 is sensitive to the elastic constants, K_{11} and K_{33}. As the elastic constant increases, a larger α_4 is required to decrease the frictional torque, thus getting the new equilibrium between the elastic and viscous torques.

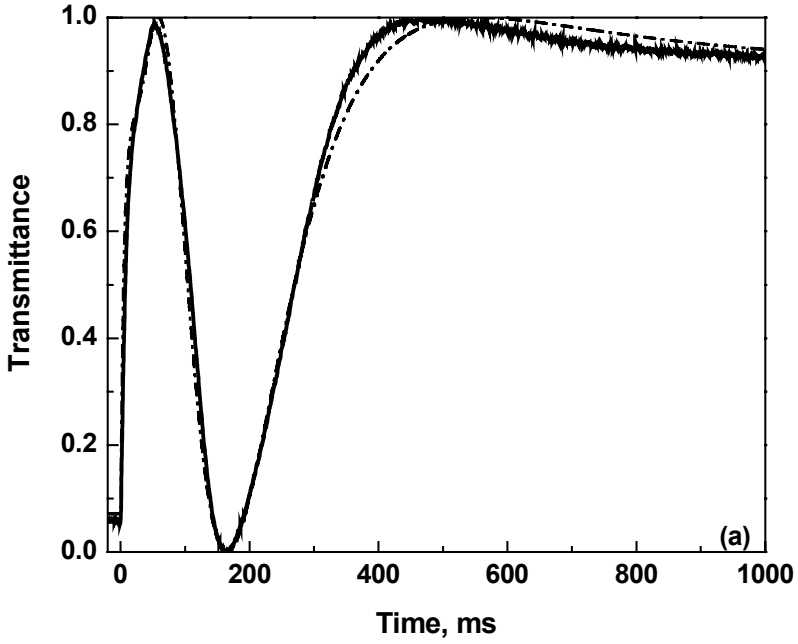

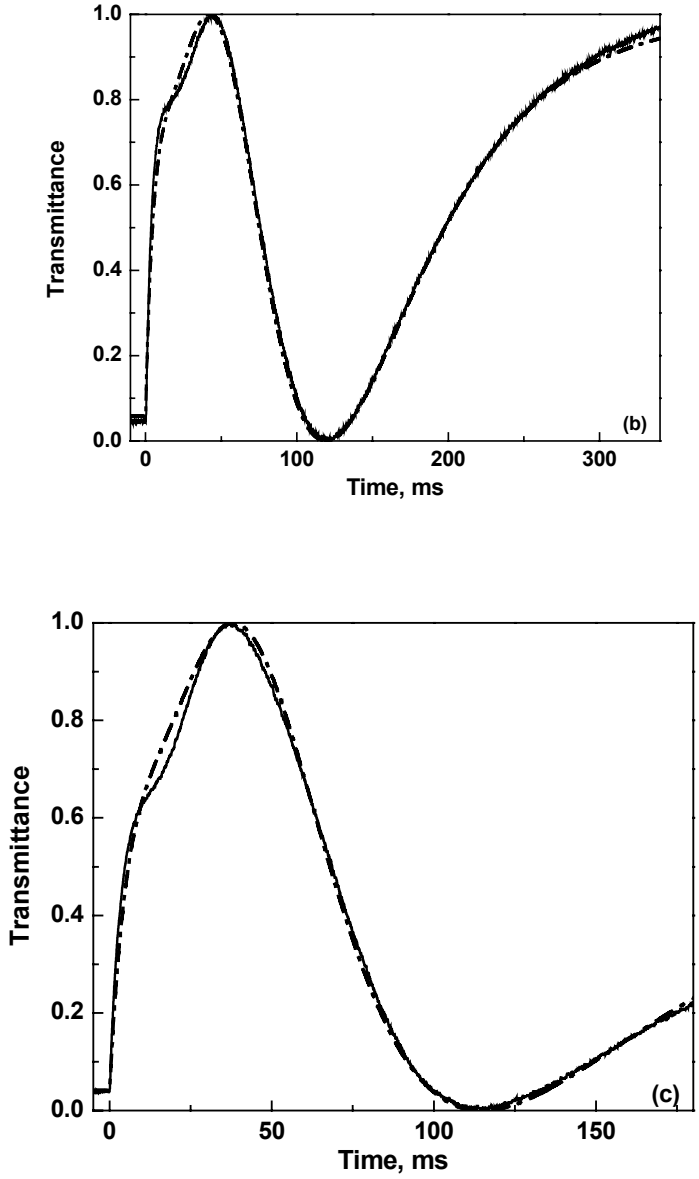

Figure 25: The transient optical dynamic responses of a homogeneous E7 LC cell at three different temperatures: (a) T = 20.3°C, (b) T =33.3°C and (c) T =46.9°C. d =13.4 μm and λ =1.55 μm. The solid lines represent the experimental results, while the dot-dashed ones are the simulation results. The parameters used for simulations are listed in Table 8.

After having optimized the α_4 values at all three temperatures, we still use Eq. (5.14) to do the fitting by only changing the activation energy of molecular diffusion. Figure 26 shows the fitting results. From the fittings, the activation energy (E) of the isotropic state can be extracted. For E7, we obtain E = 0.432 eV, which is comparable to that of MBBA (E = 0.414 eV) due to similar molecular conformations.

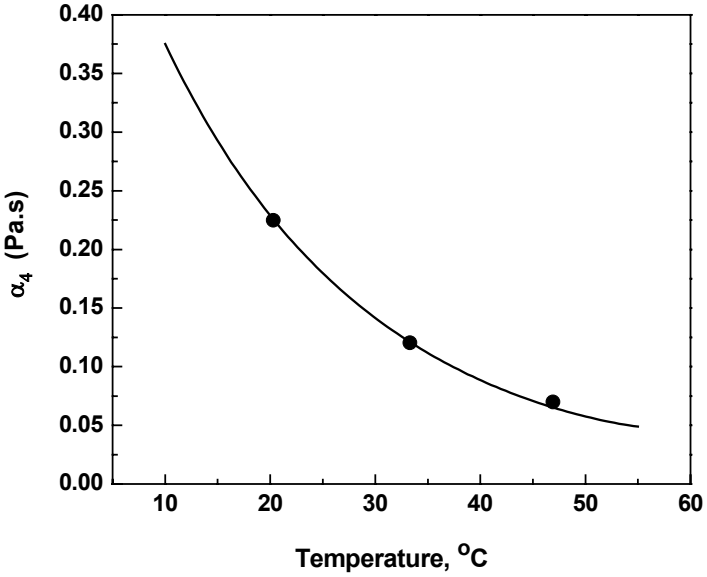

Figure 26: The temperature-dependent Leslie coefficient α_4 for E7. The solid line represents the fitting curve using Eq. (5.14) with E =0.315 eV, while the dots represent the optimal values of α_4 at each temperature.

5.4.2 UCF-2

Further to verify the essential correctness of this approach we also tried the high birefringence LC mixture, designated as UCF-2, that we formulated. Its nematic range is from

10.3 to 139.7 °C. All the parameters used for simulations are listed in Table 9. At λ =1.55 μm and T =70°C, UCF- 2 has Δn ~0.319 which is ~2X higher than that of E7 at T ~47°C. Due to the higher birefringence, the required cell gap to achieve 2π phase change is reduced in proportion. By comparing Table 9 with Table 8, we find that the α_2 (or γ_1) of E7 at T ~47°C is about the same as that of UCF-2 at T =70°C. However, UCF-2 has a much higher clearing temperature than E7, which leads to a higher K_{11}. The visco-elastic coefficient (γ_1 / K_{11}) of UCF-2 at T =70°C is ~3X smaller than that of E7 at T ~47°C. As a result, UCF-2 should have ~10X higher FoM than E7.

Table 9: Some measured and calculated LC parameters of UCF-02 at T =70 °C and λ =1.55 μm.

T (°C)	K_{11} (pN)	K_{33} (pN)	$\varepsilon_{//}$	$\Delta\varepsilon$	Δn	α_1 (mPa·s)	α_2 (mPa·s)	α_3 (mPa·s)	α_4 (mPa·s)	α_5 (mPa·s)	α_6 (mPa·s)
70	13.9	37.8	13.4	10.1	0.319	-25.9	-50.9	-0.7	72	107.9	56.3

Figure 27 plots the optical dynamic response of the UCF-02 LC cell (d =7.81μm) at T = 70°C. The simulation results (dashed line) fit very well with the experimental results (solid line). From the value of α_4, we find that E = 0.343 eV, which is ~10% higher than that of E7. Recall that E is the activation energy in the isotropic state. Although UCF-2 exhibits a lower viscosity than E7 in the nematic phase, its activation energy in the isotropic state is slightly higher than that of E7. In the isotropic state, the inter-molecular association is much weaker and the dimmers of cyano-biphenyls are separated. The moment of inertia of cyano-biphenyl is smaller than that of isothiocyanato-tolane, the major composition of UCF-2. As a result, E7 exhibits slightly smaller activation energy than UCF-2.

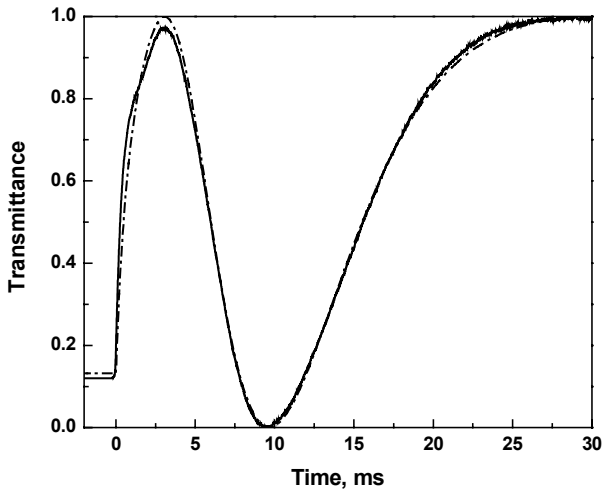

Figure 27: The transient optical dynamic responses of a homogeneous cell using UCF-02 LC mixture at T =70°C. d =7.81 μm and λ =1.55 μm. The solid line shows the experimental results and the dot-dashed lines are the simulation results. The parameters used for simulations are listed in Table 9.

5.5 Conclusion

Backflow is found to make an important impact to the response time of the phase modulator using a homogeneous LC cell. For laser beam steering at a near infrared wavelength, the required cell gap is around 5-7 μm, depending on the LC birefringence. Due to the relatively high voltage applied, the backflow takes place in the first few milliseconds. We have modified the expressions of two Leslie coefficients (α_1 and α_2) in order to extend their validity to two high birefringence LC mixtures, E7 and UCF-2. With these modifications, the simulation results agree quite well with the experimental data. The transient LC director distributions during backflow occurrence are analyzed.

CHAPTER 6: CELL GAP EFFECT ON THE DYNAMICS OF LIQUID CRYSTAL MODULATORS

6.1 Introduction

Liquid crystal spatial light modulator (SLM) has been used as a phase-only modulation for laser beam steering [36], tunable-focus lens [102]-[106], and other photonic devices[107],[108]. To obtain a large phase shift while keeping operating voltage below 10 V_{rms}, homogeneous cell (also called parallel-aligned cell) is a favorable choice. Response time of a homogeneous cell is a critical issue. To achieve a fast response time, low rotational viscosity (γ_1) LC mixtures are preferred [45],[49],[50]. Another straightforward approach is to use a thin cell gap filled with a high birefringence (Δn) and low viscosity LC mixture [16],[51]. The LC directors rise time τ_{rise} and decay time τ_{decay} are known to be proportional to d^2, where d is the cell gap. However, the theoretical derivation of this d^2 dependence is based on the small angle approximation [72]. Thus, these equations are valid only in the $V_{th} < V < \sqrt{2}V_{th}$ region, marked as Part I in Figure 28, where V is the applied voltage and V_{th} is the threshold voltage. Since the optical response time is *linearly* proportional to the LC director reorientation time [108], the corresponding optical response time is also proportional to d^2.

In the large signal regime where $V_\pi < V < V_i$, marked as Part III in Figure 28, the surface modes dominate, where V_π is the voltage corresponding to last transmittance minimum and V_i the initial voltage at the high voltage regime. As a result, both rise and decay times are fast. Moreover, the optical decay time is *independent* of the cell gap d [110],[111].

However, the optical response time in the middle voltage regime has not been studied yet. In this paper, we found that between Part I and Part III there is a region where the response time is *linearly* proportional to *d*. To validate this experimental observation, in Sec. 6.2, a complete derivation based on small angle approximation using a parallel-aligned cell is given. Experimental methods are described in Sec. 6.3. In Sec 6.4, the validity of our analytical derivation is confirmed by experimental results and the complete physical picture of optical response time as a function of cell gap in the whole voltage regime is given.

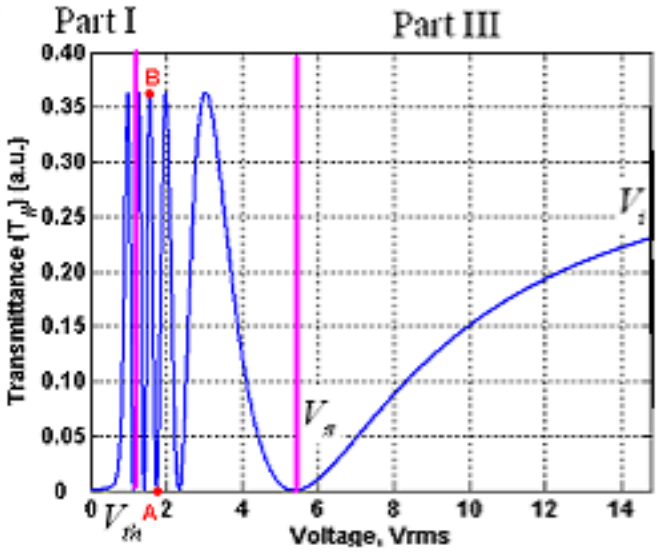

Figure 28: Simulated voltage-dependent transmittance curve of a 15.6-μm homogeneous E7 cell with 3° pretilt angle between paralleled polarizers at $\lambda = 633$ nm and 23°C, where in small signal region (Part I), small angle approximation holds well; while in high signal region (Part III), the transient nematic effect is satisfied.

6.2 Theoretical Background

The voltage-dependent transmission of a 15.6 μm, parallel-aligned E-7 cell under parallel polarizers is shown in Figure 28. Although E-7 is chosen as an example, the results should be applicable to other LC materials. Here the maximum obtainable phase difference due to the voltage-induced molecular reorientation is $\delta = 2\pi d\Delta n / \lambda$, where d is the cell gap, Δn is the birefringence, and λ is the wavelength. To illustrate the theory, let us divide the EO curve in Fig. 1 into three parts according to the biased voltage V.

6.2.1 Small Signal Region

The electro-optic effect of a parallel-alligned LC layer in the small signal regime has been studied previously [72]. When V is not far from V_{th} ($V_{th} < V < \sqrt{2}V_{th}$), the small angle approximation is hold. Then the Erickson-Leslie equation under small angle approximation can be simplified to:

$$K\frac{\partial^2\theta}{\partial z^2} + \varepsilon_0\varepsilon_r E^2\theta = \gamma_1\frac{\partial\theta}{\partial t}. \tag{6.1}$$

Under such circumstances, both rise time and decay time have simple analytical solutions, as shown in Eq. (6.1), where they are both proportional to d^2.

$$\tau_{rise} = \frac{\tau_m}{\left|(V/V_{th})^2 - 1\right|}, \tag{6.2}$$

$$\tau_{decay} = \tau_m, \tag{6.3}$$

where

$$\tau_m = \frac{\gamma_1 d^2}{K_{11}\pi^2}\frac{1}{(2m+1)^2}; \tag{6.4}$$

$$\tau_0 = \frac{\gamma_1 d^2}{K_{11}\pi^2}, \tag{6.5}$$

where *m* stands for the number of the mode. The higher order mode (surface mode) exhibits a smaller time constant. For *m* =0, the lowest spatial mode switches the slowest.

The main feature in this working scheme is that a large phase change can be achieved by a small voltage swing, which is profitable to spatial light modulators. However, this response time is relatively slow; it is proportional to γ_1 / K_{11} and d^2, where γ_1 is the rotational viscosity and K_{11} the splay elastic constant.

6.2.2 Large Single Region

The physical mechanism of the LC device operating in this regime is the transient nematic effect. The idea of the transient nematic effect is to operate the LC device at its last transmittance cycle, from the states V_i to V_π, marked as Part III in Figure 28. At this relatively high voltage region ($V >> V_{th}$), the directors are reoriented to be perpendicular to the substrates except the boundary layers. So during the free relaxation process, the surface modes (the higher order modes) dominate, as shown by the solid line in Figure 29. Thus, LC device can reach its first minimum rapidly. Moreover, Perregaux [111] and Wu [3],[110] found that the optical decay time in this regime is *independent* of the cell gap *d* by experimental method. Here we also verify it by numerical simulation, and the results will be shown in Sec. 6.4.

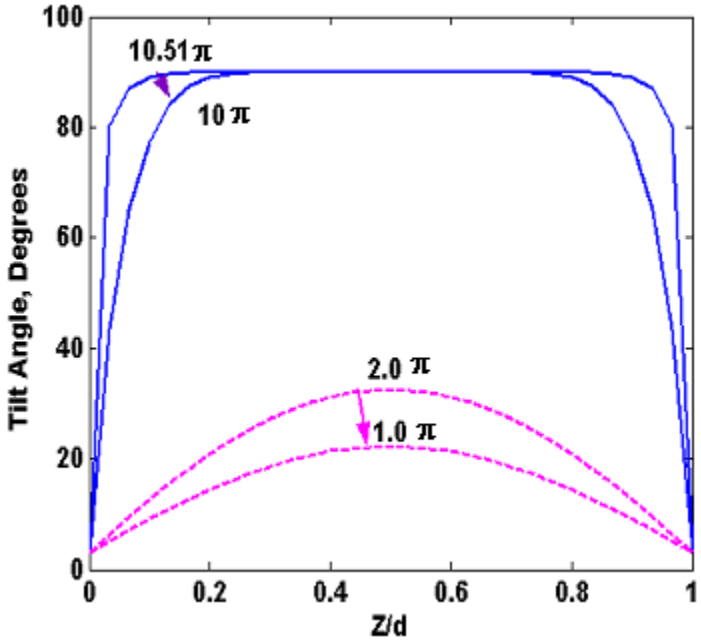

Figure 29: Director distribution of a 16.6-μm homogeneous E7 cell between paralleled polarizers at $\lambda = 633$ nm and 23°C. Solid line corresponds to its free decay from initial biased voltage V_i = 14.8 V_{rms} to its first transmittance minimum, while dotted line is its free decay from initial phase $\delta_i = 2\pi$ to 1π.

6.2.3 Middle Signal Region

To obtain a complete physical picture of optical response time as a function of cell gap in the whole voltage regime, we study the middle signal region in this chapter. Using a LC modulator to modulate light intensity, one π phase change is usually sufficient. Thus, the objective of our study is to operate the LC device between its transmittance crest (maximum) and adjacent trough (minimum). Here we only analyze its decay process. The position of the starting point corresponds to the exactly middle part in its total phase retardation of EO curve, thus, we

call it middle cycle. In Figure 28, where the total phase retardation of the LC device is ~13π, the middle cycle is from point A to B, corresponding to the LC device switching from initial phase δ_i ~6π (point A) to point B, which leads to 1π phase change.

Since the voltage-dependent intensity changes fast in the low voltage regime and saturates in the high voltage regime, indeed, the voltage V_a that corresponds to the starting point of the middle cycle (point A) is not high, which is 1.8V_{rms} as Figure 28 shows. As the total phase retardation increases, the voltage of this point will decrease. So the small angle approximation still holds in this regime. This gives us a hint to use the small angle approximation to solve the optical response time in this region. The detailed confirming numerical results will be discussed in Sec. 6.4. If the voltage is removed instantaneously from point A at t=0, the transient phase change can be approximated as [80]:

$$\delta(t) \cong \delta_i \exp(-\frac{2t}{\tau_o}) \tag{6.6}$$

where δ_i is the net phase change from V=V_a to V=0.

To find optical response time, we need to calculate the intensity change. The time-dependent normalized intensity change *I(t)* of the PA cell under crossed polarizers can be calculated using the following relationship

$$I(t) = \sin^2(\frac{\delta_i - \delta(t)}{2}). \tag{6.7}$$

Substituting Eq. (6.6) into Eq. (6.7), we obtain

$$I(t) = \sin^2\left(\frac{\delta_i(1-\exp(-\frac{2t}{\tau_o}))}{2}\right). \tag{6.8}$$

Let us assume from t_1 to t_2 the transmittance decays from point A to point B. From Eq. (6.8), I_1 and I_2 have the following forms:

$$I_1 = 0 = \sin^2\left(\frac{\delta_o(1-\exp(-\frac{2t_1}{\tau_o}))}{2}\right), \tag{6.9}$$

$$I_2 = 1 = \sin^2\left(\frac{\delta_i(1-\exp(-\frac{2t_2}{\tau_o}))}{2}\right). \tag{6.10}$$

Upon comparing Eq. (6.9) with Eq. (6.10), we conclude that

$$\frac{\delta_i}{2}\exp(-2(t_2-t_1)/\tau_0) = \frac{\delta_i-\pi}{2}. \tag{6.11}$$

Therefore, the solution of the optical decay time T_{decay} (point A→point B) is as follows:

$$T_{decay} = t_2 - t_1 = \frac{\tau_o}{2}\ln\left(\frac{\delta_i}{\delta_i-\pi}\right). \tag{6.12}$$

Meanwhile, the initial phase δ_i can be expressed as:

$$\delta_i = \delta_0 - \text{int}(\delta_0/2\pi)\pi. \tag{6.13}$$

Substituting Eq. (6.13) to Eq. (6.12), we can obtain the optical decay time T_{decay} as a function of the total phase retardation δ_0 as:

$$T_{decay} = \frac{\tau_o}{2}\ln\left(1+\frac{1}{\delta_0/\pi - \text{int}(\delta_0/2\pi) - 1}\right). \tag{6.14}$$

If the following assumption is made: δ_0 is large so that $\text{int}(\delta_0/2\pi)+1 \approx \delta_0/2\pi$, Eq. (6.14) can be greatly simplified as:

$$T_{decay} = \frac{\gamma_1 d}{K_{11}\pi^2}\frac{\lambda}{2\Delta n}. \quad (6.15)$$

Equation (6.15) indicated that the optical response time T_{decay} in the middle cycle is *linearly* proportional to *d*. In the following, we will verify our derivation by comparing the experimental and simulation results.

6.3 Experiment

We prepared a set of homogeneous cells with different thickness using a commercial LC material E7. The cell gaps were determined from transmitted interference fringes through a spectrophotometer and found to be 7.8, 10.7 and 16.2 μm. We measured and analyzed the electro-optic characteristics of the LC cells at $\lambda = 633$ nm through a LabVIEW data acquisition system. To study the optical response times in different voltage regimes, the LC cell was initially biased at V_i. During the relaxation process, the voltage was removed at t =0 and the optical response monitored by a photodiode detector and displayed by a digital oscilloscope.

6.4 Results and Discussion

To verify our derivation in Eq. (6.15), we numerically solve the Erickson-Leslie equation using the finite element method (FEM) [53]. To compare with experimental results, we also use E7 in our simulations.

6.4.1 Middle Signal Region

The simulated transient phase change in the middle cycle of a 10-μm homogeneous E7 cell with 3° pretilt angle at T = 23°C and $\lambda = 633$ nm released from $V_i = 1.815$ V_{rms} is depicted

in Figure 30, where the gray line shows the simulated phase change, while the red dash line is the fitting data in Eq. (6.6). The initial phase change δ_0 is 4π. It is evident that the small angle approximation holds well in this regime, even though V_i =1.8 V_{th}. Thus, the assumption of our derivation is validated. Therefore, we can use the small angle approximation to solve the optical response time in this region as presented in Sec. 6.2.

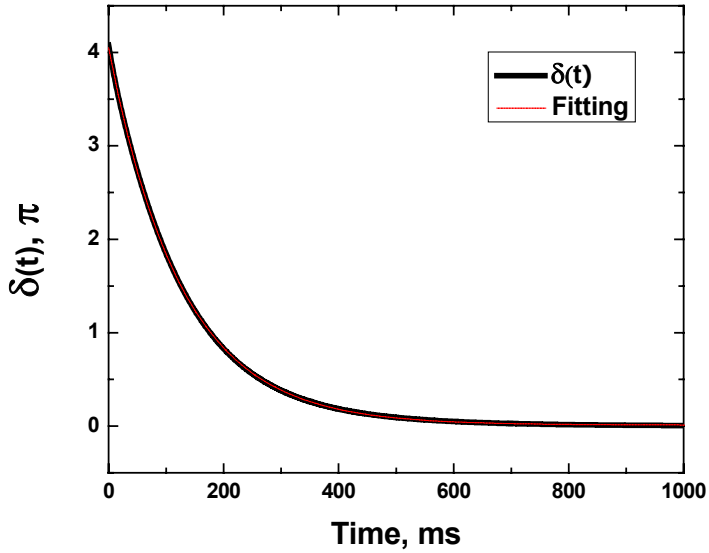

Figure 30: Simulated transient phase change in the middle cycle of a 10-μm homogeneous E7 cell with 3° pretilt angle at T = 23°C and λ =633 nm released from V_i =1.815 V_{rms}. The gray line shows the simulated transient phase change, while the red dash line is the fitting data using Eq. (6.6). Thus, the transient phase change in the middle cycle follows the small angle approximation.

We also measured the optical decay time t_{op} in this region with these three cells. The measured results are plotted in Figure 31 (filled square). Also included in Figure 31 for comparison are the calculation results from Eq. (6.15) (open squares). The measured results agree well with the theoretical expectation. It is obvious that in this part the optical response time is *linearly* proportional to *d*.

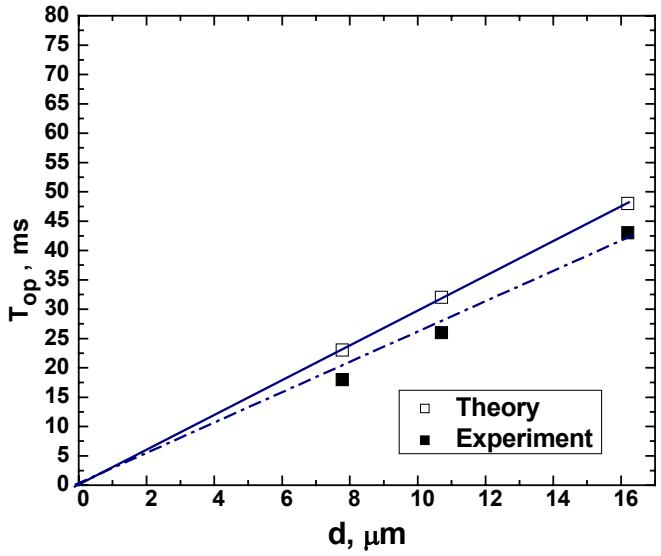

Figure 31: Measured and calculated optical decay times in the middle cycle as a function of the cell gap, where the filled and the empty squares show the experimental and calculation results in Eq. (6.15), respectively.

6.4.2 Large Signal Region

Our study not only predict the theory of optical response time in the middle cycle, but also verify the transient nematic effect in the large signal region and small angle approximation in the small signal region. Here we only show some results in the large signal region.

In Figure 32, the above light blue line shows the experimental optical decay curve of a 10.7-μm homogeneous E7 cell between crossed polarizers at $\lambda = 633$ nm and 23°C, the bottom dark blue curve is the driving square wave which initial biased at 14.8 V_{rms} and dropped to 0 at t =0. The optical response time t_{op} of this cell from V_i =14.8 V_{rms} at the last cycle (from t =0 to first maximum) is ~2.6 ms. This result agrees well with the published value [110].

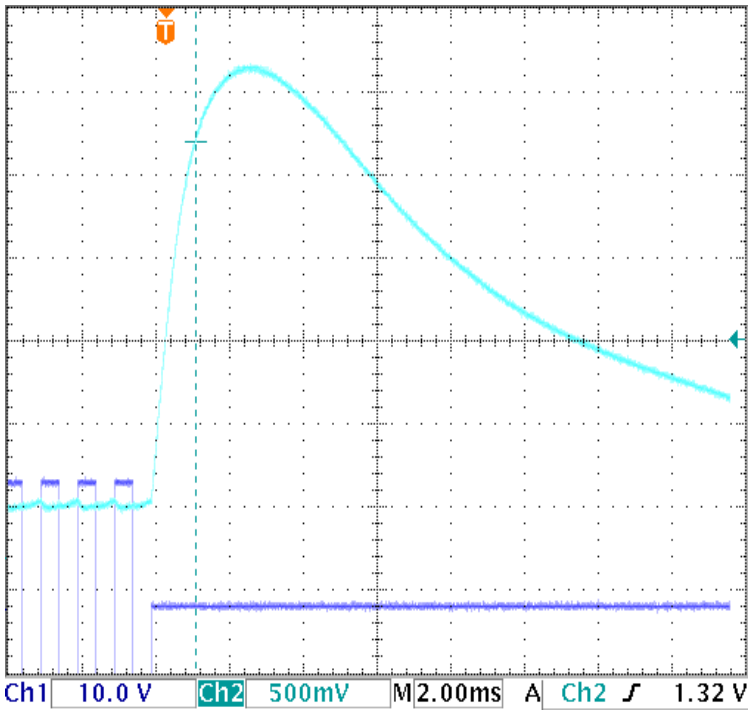

Figure 32: Experimental optical decay curve of a 10.7-μm homogeneous E7 cell between crossed polarizers at T =23°C and $\lambda = 633$ nm from the initial bias voltage V_i =14.8 V_{rms} (light blue line).

Figure 33 compares the results of the optical response time in the last cycle, where the red squares show the experimental optical response times of these three cells released from V_i =1.815 V_{rms}, while the black diamonds give the simulation data. It is clear that the simulation

data match the experimental results quite well. Furthermore, beyond d >10 μm, t_{op} is insensitive to d as indicated in Sec. 6.2.

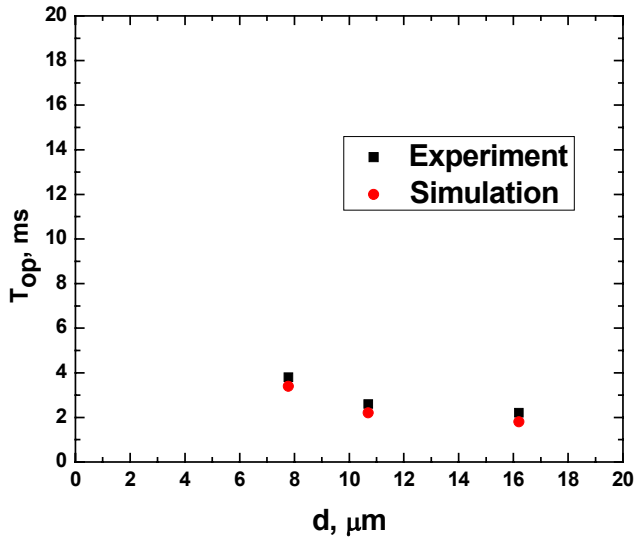

Figure 33: Optical response time t_{op} at the last cycle is as a function of the cell gap. LC used is E7 at $T = 23°C$ and $\lambda = 633$ nm. Beyond d >10 μm, t_{op} is insensitive to d as expected in Sec. 6.2.

Table 10 summarizes the measurement results of the optical response time t_{op} of these three cells at different voltage regimes. The optical response time in the last cycle is initially biased at V_i =19.5 V_{rms}. Let us look at column by column. In the last cycle, the decay time is really fast, due to the surface mode effect. Moreover, the optical response time is independent of the cell gap. In the middle cycle, the measured response time, as the filled square plotted in Figure 33, is *linearly* proportional to the cell gap. In the first cycle, because of the smaller elastic torque, the optical response time is relatively slow. Furthermore, the measured optical response time is proportional to d^2 as predicted by the theory.

Table 10: Measured optical response times of three various cells d = 7.78, 10.7 and 16.2 μm in different cycles. The optical response time in the last cycle is initially biased at V_i=19.5 V_{rms} at t =0 ms.

d (μm)	First Cycle (ms)	Middle Cycle (ms)	Last Cycle (ms)
16.2	840	43	2.2
10.7	250	26	2.4
7.78	80	18	2.5

6.5 Conclusion

We have analyzed theoretically and confirmed experimentally that the optical response time in the middle phase cycle of the EO curve is *linearly* proportional to d. The analytical solution of the optical response time is derived based on the small angle approximation. The confirming experimental and the simulation results agree well with the theoretical expectation. Therefore, in the whole voltage regime, the physical picture of optical response time as a function of cell gap is completed. This analysis is useful for understanding the grayscale switching behaviors of the LC phase modulators. This approach will be helpful to achieve the fast response time in phase modulators using a thicker cell gap or double cell gaps. Considering the birefringence dispersion of LC mixtures, it is more attractive in the low wavelength regime, especially in the visible light.

CHAPTER 7: SUMMARY

This dissertation investigates optical response time with objectives to meet challenges in liquid crystal applications for display and photonic systems. From the research topics covered here, the dissertation can be categorized into two parts.

The first three introductory chapters present the motivation of our research work and simulation methodologies of LC that we used in our studies. The second part, Chapter 4-6, is devoted to various novel electro-optic effects that related to optical response time of nematic LC materials. The major emphasis is to explain the physical nature of the phenomena.

One major work in this thesis is that we give the rigorous analytical solutions of the correlation function between the LC director response time and its consequent optical response times (both rise and decay) of a vertically aligned nematic LC cell, which is based on the small angle approximation. Pretilt angle effect on the LC dynamics is studied, and we find that a modified rotational viscosity should be used to justify this effect. Grayscale switching is also analyzed numerically. This work successfully fills the gap in the literature on LCD switching.

Backflow is an important effect related to LC response time while the applied voltage is high. We analyze the backflow effect using a homogeneous LC cell in an infrared wavelength. Due to the relatively high voltage applied in optical phased array (OPA), the backflow takes place in the first few milliseconds, which subsequently affects the LC response time. However, the complete set of Leslie viscosity coefficients, which are critical to investigate the dynamic response of LC devices with backflow, are only available for MBBA. A new effective approach to estimate the Leslie coefficients of LC mixtures based on MBBA data is proposed. Using this method, the material's Leslie coefficients can be extracted based on its order parameter. The

simulation results agree with experiment very well. This method supplies a useful tool for analyzing the dynamic response with backflow, which can be used to obtain accurate optical response time under a high biased voltage.

Cell gap is critical to LC response time. Usually a thinner cell gap is chosen to achieve faster response time since normally both rise and decay times are known to be proportional to d^2. However, they are valid only in the $V_{th} < V < \sqrt{2}V_{th}$ region. In the large signal region, where $V_{\pi} < V < V_i$, the surface modes dominate and the optical decay time is *independent* of *d*. We find that between these two extremes, the response time is *linearly* proportional to *d*. Our analytical derivation is confirmed by experimental results. Therefore, in the whole voltage region, the whole physical picture of the optical response time as a function of the cell gap is completed. This analysis is useful for understanding the grayscale switching behaviors of the LC phase modulators. Understanding the cell gap effect on phase modulators, we can effectively reduce the response time by using a thick cell or double cells to achieve the specific phase retardation for a given wavelength.

In conclusion, this dissertation has solved some important issues related to LC response time and developed useful tools for scientists and engineers to simulate the LC dynamics.

LIST OF REFERENCES

[1] A. Spadło, R. Dąbrowski, M. Filipowicz, Z. Stolarz, J. Przedmojski, S. Gauza, Y. H. Fan and S. T. Wu, "Synthesis, mesomorphic and optical properties of isothiocyanatotolanes," *Liq. Cryst.* **30**, 191-198 (2003).

[2] S. Gauza, H. Wang, C. H. Wen, S. T. Wu, A. J. Seed and R. Dąbrowski, "High birefringence isothiocyanato tolane liquid crystals," *Jpn. J. Appl. Phys.* Pt. 1, **42**, 3463-3466 (2003).

[3] S. T. Wu and C. S. Wu, "High-speed liquid-crystal modulators using transient nematic effect," *J. Appl. Phys.* **65**, 527-532 (1989).

[4] S. Nagata, E. Takeda, Y. Nanno, T. Kawaguchi, Y. Mino, A. Otsuka, and S. Ishihara, "Capacitively coupled driving of TFT- LCD," *SID Digest* **20**, 242-245 (1989).

[5] K. Sekiya and H. Nakamura, "Eye-trace integration effect on the perception of moving pictures and a new possibility for reducing blur on hold-type displays," *SID Digest* **33**, 930-933 (2002).

[6] H. Okumura, M. Baba, K. Taira and A. Kinno, "Advanced-level adaptive overdrive (ALAO) method applicable to full HD-LCTVs," *SID Digest* **33**, 68-71 (2002).

[7] B. W. Lee, D. Sagong, and G. Jeong, "LCD: How fast is enough," *SID Digest* **32**, 1106-1109 (2001).

[8] B. W. Lee, C. Park, S. Kim, M. Jeon, J. Heo, D. Sagong, J. Kim, and J. Souk, "Reducing gray-level response to one frame: dynamic capacitance compensation," *SID Digest* **32**, 1260-1263 (2001).

[9] T. Konno, T. Miyashita, T. Uchida, "OCB-cell using polymer stabilized bend alignment," *Asia Display* 581 (1995).

[10] M. Xu, D. K. Yang, P. J. Bos, X. Jin, "Very high pretilt alignment and its application in Pi-cell LCDs," *SID Digest* **29**, 139-142 (1998).

[11] M. Noguchi, H. Nakamura, "The phase initialization in the Pi-cell," *SID Digest* **28**, 739-742 (1997).

[12] V. Ezhov, S. Studenzov, S. Belyaev, V. Chigrinov, N. Malimonenko and a. Miroshin, "3-D vision based on fast nematic liquid-crystal shutters," *SID Digest* **27**, 143-144 (1996).

[13] C. H. Lee, H. S. Chang, J. J. Lyu, K. H. Kim and J. H. Souk, "A high-performance 17.0-in. SVGA OCB panel with fast initial bend transition," *SID Digest* **33**, 570-573 (2002).

[14] M. Xu and D. K. Yang, "Dual frequency cholesteric light shutters," *Appl. Phys. Lett.* **70**, 720-722, (1997).

[15] S. C. Jain, K. S. Balakrishnan and S. CHANDRA, "Effect of the pretilt angle and temperature on the multiplexing limits of dual frequency addressed TN-LC cell," *Jpn. J. Appl. Phys.* **26**, 336-340 (1987).

[16] Y. H. Fan, Y. H. Lin, H. Ren, S. Gauza and S. T. Wu, "Fast-response and scattering-free polymer network liquid crystals for infrared light modulators," *Appl. Phys. Lett.* **84**, 1233-1235 (2004).

[17] D. J. Channin, "Triode optical gate: A new liquid crystal electro-optic device," *Appl. Phys. Lett.* **26**, 603-605 (1975).

[18] C. Y. Xiang, J. X. Guo, X. W. Sun, X. J. Yin and G. J. Qi, "A fast response, three-electrode liquid crystal device," *Jnp. J. Appl. Phys.* **42**, L763-L765 (2003).

[19] C. Y. Xiang, X. W. Sun, J. X. Guo, X. J. Yin and G. J. Qi, "The electro-optic properties of a fast response, three-electrode liquid crystal device," *Jnp. J. Appl. Phys.* **43**, 1068-1072 (2004).

[20] C. Y. Xiang, X. W. Sun and X. J. Yin, "The electro-optic properties of a vertically aligned fast response liquid crystal display with three-electrode driving," *J. Phys. D Appl. Phys.* **37**, 994-997 (2004).

[21] C. Y. Xiang, X. W. Sun and X. J. Yin, "Fast response wide viewing angle liquid crystal cell with double-side fringe-field switching," *Appl. Phys. Lett.* **83**, 5154-5156 (2003).

[22] C. Y. Xiang and X. W. Sun, "Vertically aligned liquid crystal light valve controlled by double-side fringe-field switching with memory effect," *Appl. Phys. Lett.* **84**, 4397-4399 (2004).

[23] H. Pan, X. Feng, and S. Daly, "Quantitative analysis of LCD motion blur and performance of existing approaches," *SID Digest* **36**, 1590-1593 (2005).

[24] T. Nose, M. Suzuki, D. Sasaki, M. Imai and H. Hayama, " A black stripe driving scheme for displaying motion pictures on LCDs," *SID Digest* **32**, 994-997 (2001).

[25] N. Fisekovic, T. Nauta, H. Cornelissen and J. Bruinink, "Improved motion picture quality of AM-LCDs using scanning backlight," *Int. Disp.Work.*1637-1640 (2001).

[26] T. Furuhashi and K. Kawabe, J. Hirakata, Y. Tanaka, and T. Sato, "High quality TFT-LCD system for moving picture," *SID Digest* **33**, 1284-1287 (2002).

[27] B. W. Lee, K. Song, D. J. Park, Y. Yang, U. Min, S. Hong, C. Park, M. Hong, and K. Chung, "Mastering the moving image: refreshing TFT-LCDs at 120 Hz," *SID Digest* **36**, 1583-1586 (2005).

[28] M. A. Klompenhouwer and L. J. Velthoven, "LCD motion blur reduction with motion compensated inverse filtering," *SID Digest* **35**, 1106-1109 (2004).

[29] I. C. Khoo and S. T. Wu, *Optics and Nonlinear Optics of Liquid Crystals* (World Scientific, Singapore, 1993).

[30] M. Wand, W. N. Thurmes, R. T. Vohra, and K. M. More, "Advances in ferroelectric liquid crystals for microdisplay applications," *SID Digest* **27**, 157-161 (1996).

[31] T. Ogawa, S. Fujita, K. Lwai, H. Koseki, "The trends of reflective LCDs for future electronic paper," *SID Digest* **29**, 217-220 (1998).

[32] S. T. Wu and D. K. Yang, *Reflective Liquid Crystal Displays* (Wiley, New York, 2001).

[33] J. L. Fergason, "Polymer encapsulated nematic liquid crystal storage displays," *SID Digest* **16**, 68-71 (1985).

[34] R. L. Sutherland, V.P. Tondiglia, and L.V. Natarajan, "Electrically switchable volume gratings in polymer-dispersed liquid crystals," *Appl. Phys. Lett.* **64**, 1074-1076 (1994).

[35] J. Qi, L. Li, M. DeSarkar, G. Crawford, "Optical characterization and modeling of holographically formed polymer-dispersed liquid crystals for reflective-display applications," *SID Digest* **33**, 538-541 (2002).

[36] P. F. McManamon, T. A. Dorschner, D. L. Corkum, L. Friedman, D. S. Hobbs, M. Holz, S. Liberman, H. Q. Nguyen, D. P. Resler, R. C. Sharp, and E. A. Watson, "Optical phased array technology," *Proc. IEEE* **84**, 268-298 (1996).

[37] M. F. Vuks, "Determination of the optical anisotropy of molecules of aromatic compounds from the double refraction of crystals," *Opt. Spectrosk* **20**, 644-651 (1966).

[38] S. T. Wu, "Birefringence dispersions of liquid crystals," *Phys. Rev. A* **33**, 1270-1274 (1986).

[39] F. Guerin, J. M. Chappe, P. Joffre, and D. Dolfi, "Modeling, synthesis and characterization of a millimeter-wave multilayer microstrip liquid crystal phase shifter," *Jpn. J. Appl. Phys*. **36**, 4409-4413 (1997).

[40] K. C. Lim, J. D. Margerum, and A. M. Lackner, "Liquid crystal millimeter wave electronic phase shifter," *Appl. Phys. Lett.* **62**, 1065-1067 (1993).

[41] S. T. Wu, C. S. Wu, "A three-band model for liquid-crystal birefringence dispersion," *J. Appl. Phys*. **66,** 5297-5301 (1989).

[42] S. T. Wu, C. S. Wu, M. Warenghem, and M. Ismaili, "Refractive-index dispersions of liquid-crystals," *Opt. Eng*. **32**, 1775-1780 (1993).

[43] J. Li and S. T. Wu, "Extended Cauchy equations for the refractive indices of liquid crystals," *J. Appl. Phys*. **95**, 896-901 (2004).

[44] J. Li, S. Gauza, and S. T. Wu, "Temperature effect on liquid crystal refractive indices," *J. Appl. Phys*. **96**, 19-24 (2004).

[45] J. Li, S. Gauza, and S. T. Wu, "High temperature-gradient refractive index liquid crystals," *Opt. Express* **12**, 2002-2010 (2004).

[46] S.Naemura, "Recent progress in LC-materials for AMLCDs," *18th Intel. Disp. Rese. Conf.* 3-13 (1998).

[47] W. Maier and G. Meier, "A simple theory of the dielectric characteristics of homogeneous oriented crystalline-liquid phases of the nematic type," *Z. Naturforsch. Teil A* **16**, 262 (1961).

[48] S. Kibe, N. Hattori, M. Ushioda, H. Yamamoto, and S. Matsui, "Novel liquid-crystal materials for AMLCDs," *J. SID* **11**, 449-455 (2003).

[49] T. Geelhaar, K. Tarumi, and H. Hirschmann, "Trends in LC materials," *SID Digest* **27**, 167-172 (1996).

[50] Y. Goto, T. Ogawa, S. Sawada, and S. Sugimori, "Fluorinated liquid-crystals for active matrix displays," *Mol. Cryst. Liq. Cryst.* **209**, 1-7 (1991).

[51] Y. Lu, F. Du, Y. H. Lin, S. T. Wu, "Variable optical attenuator based on polymer stabilized twisted nematic liquid crystal ," *Opt. Express* **12**, 1221-1227 (2004).

[52] N. Mizoshita, K. Hanabusa, and T. Kato, "Fast and high-contrast electro-optical switching of liquid-crystalline physical gels: formation of oriented microphase-separated structures," *Adv. Funct. Mater.* **13**, 313-317 (2003).

[53] Y. H. Fan, H. Ren and S. T. Wu, "Normal mode anisotropic liquid crystal gels," *Appl. Phys. Lett.* **82**, 2945-2947 (2003).

[54] J. E. Akin, *Finite Elements for Analysis and Design* (Academic Press, San Diego, 1994).

[55] A. Taflove, S. C. Hagness, *Computational Electrodynamics: the Finite-Difference Time-Domin Method* (Artech House, Boston, 2000).

[56] W. H. Hayt, Jr. J. A. Buck, *Engineering Electromagnetics* (McGraw-Hill Higher Education, New York, 2001).

[57] A. Lien, "A detailed derivation of extended Jones matrix representation for twisted nematic liquid crystal displays," *Liq. Cryst.* **22**, 171-175 (1997).

[58] M. V. K. Chari, S. J. Salon, *Numerical Methods in Electromagnetism* (Academic Press, San Diego, 2000).

[59] G. Panasyuk and D. W. Allender, "Approximate description of the three dimensional director and electric field in a liquid crystal display at a high voltage," *J. Appl. Phys.* **87**, 649-657 (2000).

[60] J. E. Anderson, C. Titus, P. Watson, and P. J. Bos, "Significant speed and stability increases in multi-dimensional director simulations," *SID Digest* **31**, 906-909 (2000).

[61] R. C. Jones," A new calculus for the treatment of optical systems. IV," *J. Opt. Soc. Am.* **32**, 486-493 (1942).

[62] D. W. Berreman, "Optics in stratified and anisotropic media: 4×4 matrix formulation," *J. Opt. Soc. Am.* ***62***, 502-510 (1972).

[63] D. W. Berreman, "Optics in smoothly varying anisotropic planar structure: application to liquid crystal twist cells," *J. Opt. Soc. Am.* **63**, 1374-1380 (1973).

[64] H. Wohler, G. Hass, M. Fritsch, and D. A. Mlynski, "Faster 4×4 matrix method for uniaxial inhomogeneous media," *J. Opt. Soc. Am. A* **5**, 1554-1557 (1988).

[65] P. Yeh, "Extended Jones matrix method," *J. Opt. Soc. Am.* 7**2**, 507-513 (1982).

[66] C. Gu and P. Yeh, "Extended Jones matrix method II," *J. Opt. Soc. Am. A* **10**, 966-973 (1993).

[67] A. Lien, "Extended Jones matrix representation for the twisted nematic liquid-crystal display at oblique incidence," *Appl. Phys. Lett.* **57**, 2767-2769 (1990).

[68] F. H. Yu and H. S. Kwok, "Comparison of extended Jones matrices for twisted nematic liquid-crystal displays at oblique angles of incidence," *J. Opt. Soc. Am. A* **16**, 2772-2780 (1999).

[69] Y. Huang, T. X. Wu, and S. T. Wu, "Simulations of liquid-crystal Fabry–Perot etalons by an improved 4×4 matrix method," *J. Appl. Phys.* **93**, 2490-2495 (2003).

[70] S. Suyama, M. Date, H. Takada, "Three-dimensional display system with dual-frequency liquid-crystal varifocal lens," *Jpn. J. Appl. Phys.* **39**, 480-484 (2000).

[71] K. Yoshino, Y. Shimoda, Y. Kawagishi, K. Nakayama, and M. Ozaki, "Temperature tuning of the stop band in transmission spectra of liquid-crystal infiltrated synthetic opal as tunable photonic crystal," *Appl. Phys. Lett.* **75**, 932-934 (1999).

[72] E. Jakeman and E. P. Raynes, "Saturation broadening by inhomogeneous fields," *Phys. Lett. A* **39**, 69-77 (1972).

[73] S. T. Wu, "Phase retardation dependent optical response time of parallel-aligned liquid crystals," *J. Appl. Phys.* **60**, 1836-1838 (1986).

[74] M. F. Schiekel and K. Fahrenschon, "Deformation of nematic liquid crystals with vertical orientation in electrical fields," *Appl. Phys. Lett.* **19**, 391-393 (1971).

[75] A. Takeda, S. Kataoka, T. Sasaki, H. Chida, H. Tsuda, K. Ohmuro, Y. Koike, T. Sasabayashi, and K. Okamoto, "A super-high image quality multi-domain vertical alignment LCD by new rubbing-less technology," *SID Digest* **29**, 1077-1080 (1998).

[76] J. O. Kwag, K. C. Shin, J. S. Kim, S. G. Kim, and S. S. Kim, "Implementation of a new wide-viewing-angle mode for TFT-LCDs," *SID Digest* **31**, 256-259 (2000).

[77] R. D. Sterling and W. P. Bleha, "D-ILA^{TM} technology for electronic cinema," *SID Digest* **31**, 310-313 (2000).

[78] J. L. Erickson, "Conservation laws for liquid crystals," *Trans. Soc. Rheol.* **5**, 23 (1961).

[79] F. M. Leslie, "Some constitutive equations for liquid crystals," *Arch. Ration. Mech. Anal.* **28**, 265-283 (1968).

[80] V. Freedericksz and V. Zolina, "Forces causing the orientation of an anisotropic liquid," *Trans. Faraday Soc.* **29**, 919 (1933).

[81] S. T. Wu and C. S. Wu, "Experimental confirmation of the Osipov-Terentjev theory on the viscosity of nematic liquid crystals," *Phys. Rev. A* **42**, 2219-2227 (1990).

[82] L. M. Blinov, *Electro-Optical and Magneto-Optical Properties of Liquid Crystals* (Wiley & Sons, New York, 1983).

[83] J. Jing, *The Finite Element Method in Electromagnetics* (Wiley & Sons, New York, 1993).

[84] V. V. Belyaev and V. G. Chigrinov, "Figure of merit of liquid crystalline materials for optically addressed spatial modulators," *Appl. Opt.* **32**, 141-146 (1993).

[85] J. M. Geary, J. W. Goodby, A. R. Kmetz, and J. S. Patel, "The mechanism of polymer alignment of liquid-crystal materials," *J. Appl. Phys.* **62**, 4100-4108 (1987).

[86] D. S. Seo, S. Kobayashi, and M. Nishikawa, "Study of the pretilt angle for 5CB on rubbed polyimide films containing trifluoromethyl moiety and analysis of the surface atomic concentration of F/C(%) with an electron spectroscope for chemical analysis," *Appl. Phys. Lett.* **61**, 2392-2394 (1991).

[87] S. T. Wu, U. Efron and L. D. Hess, "Infrared birefringence of liquid crystals," *Appl. Phys. Lett.* **44**, 1033-1035 (1984).

[88] C. Z. Van Doorn, "Dynamic behavior of twisted nematic liquid-crystal layers in switched fields," *J. Appl. Phys.* **46**, 3738-3745 (1975).

[89] D. W. Berreman, "Liquid-crystal twist cell dynamics with backflow," *J. Appl. Phys.* **46**, 3746-3751 (1975).

[90] H. Kneppe, F. Schneider, and N. K. Sharma, "Rotational viscosity γ_1 of nematic liquid crystals," *J. Chem. Phys.* **77**, 3203-3208 (1982).

[91] H. Imura and K. Okano, "Temperature dependence of the viscosity coefficients of liquid crystals," *Jpn. J. Appl. Phys.* **11**, 1440-1445 (1972).

[92] H. Schmiedel, R. Stannaurius, M. Grigutsch, R. Hirning, J. Stelzer, and H. R. Trebin, "Determination of viscoelastic coefficients from the optical transmission of a planar liquid crystal cell with low-frequency modulated voltage," *J. Appl. Phys.* **74**, 6053-6057 (1993).

[93] J. Kelly, S. Jamal, and M. Cui, "Simulation of the dynamics of twisted nematic devices including flow," *J. Appl. Phys.* **86**, 4091-4095 (1999).

[94] N. Konforti, E. Marom and S. T. Wu, "Phase-only modulation with twisted nematic liquid-crystal spatial light modulators," *Opt. Lett.* **13**, 251-253 (1988).

[95] W. H. De Jeu, *Physical Properties of Liquid Crystalline Materials* (Golden and Breach, New York, 1980).

[96] I. Haller, "Thermodynamic and static properties of liquid crystals," *Prog. Solid State Chem*. **10**, 103-110 (1975).

[97] O. Parodi, "Stress tensor for a nematic liquid crystal," *J. Phys*. **31**, 581-584 (1970).

[98] S. T. Wu and C. S. Wu, "Rotational viscosity of nematic liquid crystals: A critical examination of existing models," *Liq. Cryst.* **8**, 171 (1990).

[99] S. T. Wu, U. Efron, and L. D. Hess, "Birefringence measurements of liquid crystals," *Appl. Opt.* **23**, 3911-3915 (1984).

[100] S. T. Wu, A. M. Lackner, and U. Efron, "Optimal operation temperature of liquid crystal modulators," *Appl. Opt.* **26**, 3441-3445 (1987).

[101] Y. H. Lin, H. Ren, Y. H. Wu, X. Liang, and S. T. Wu, "Pinning effect on the phase separation dynamics of thin polymer-dispersed liquid crystals," *Opt. Express* **13**, 468-474 (2005).

[102] S. Sato, "Liquid-crystal lens-cells with variable focal length," *Jpn. J. Appl. Phys.* **18**, 1679-1684 (1979).

[103] G. D. Love, J. V. Major, and A. Purvis, "Liquid-crystal prisms for tip-tilt adaptive optics," *Opt. Lett.* **19**, 1170-1172 (1994).

[104] V. V. Presnyako, K. E. Asatryan, and T. V. Galstian, "Polymer-stabilized liquid crystal for tunable microlens applications," *Opt. Express* **10**, 865-870 (2002).

[105] H. Ren and S. T. Wu, "Inhomogeneous nanoscale polymer-dispersed liquid crystals with gradient refractive index," *Appl. Phys. Lett.* **81**, 3537-3539 (2002).

[106] H. Ren and S. T. Wu, "Tunable electronic lens using polymer network liquid crystals," *Appl. Phys. Lett.* **82**, 22-24 (2003).

[107] J. Chou, Y. Han, and B. Jalali, "Adaptive RF-photonic arbitrary waveform generator," *IEEE Photo. Tech. Lett.* **15**, 581-583 (2003).

[108] A. Sneh and K. M. Johnson, "High-speed continuously tunable liquid crystal filter for WDM networks," *J. Light. Tech.* **14**, 1067-1080 (1996).

[109] H. Wang, T. X. Wu, X. Zhu and S. T. Wu, "Correlations between liquid crystal director reorientation and optical response time of a homeotropic cell," *J. Appl. Phys.* **95**, 5502-5508 (2004).

[110] S. T. Wu and C. S. Wu, "Small angle relaxation of highly deformed nematic liquid crystals," *Appl. Phys. Lett.* **53**, 1794-1796 (1988).

[111] A. E. Perregaux, "Transient state liquid crystal image bar for electrophotographic printers," U. S. Patent 4,595,259 (1986).

LIST OF PUBLICATIONS

Referred Journals:

1. H. Wang, X. Nie, T. X. Wu, and S. T. Wu, "Cell gap effect on the dynamics of liquid crystal phase modulators," *Mol. Cryst. Liq. Cryst.* (Accepted, Nov. 2005).
2. H. Wang, T. X. Wu, S. Gauza, J. R. Wu and S. T. Wu, "A method to estimate the Leslie coefficients of liquid crystals based on MBBA data," *Liq. Cryst.* (Accepted, Sept. 2005).
3. Y. H. Fan, H. Ren, X. Liang, H. Wang, and S. T. Wu, "Liquid crystal microlens arrays with switchable positive and negative focus lengths," *J. Display Technology* **1**, 151-156 (Sept. 2005).
4. X. Nie, Y. H. Lin, T. X. Wu, H. Wang, Z. Ge, and S. T. Wu, "Polar anchoring energy measurement of vertically-aligned liquid crystal cells," *J. Appl. Phys.* **98**, 013516 1-5 (July 1, 2005).
5. X. Liang, Y. Q. Lu, Y. H. Wu, F. Du, H. Wang, and S. T. Wu, "Dual-frequency addressed variable optical attenuator with submillisecond response time," *Jpn. J. Appl. Phys.* **44**, 1292-1295 (March 8, 2005).
6. C. H. Wen, S. Gauza, J. Li, H. Wang, and S. T. Wu, "High contrast homeotropic alignment of difluoro-tolane liquid crystals," *Liq. Cryst.* **32**, 643-649 (May, 2005).
7. H. Wang, T. X. Wu, X. Zhu, and S. T. Wu, "Correlations between liquid crystal director reorientation and optical response time of a homeotropic cell," *J. Appl. Phys.* **95**, 5502-5508 (May 15, 2004).

8. S. Gauza, H. Wang**,** C. H. Wen, S. T. Wu, A.J. Seed, and R. Dabrowski, "High birefringence isothiocyanato tolane liquid crystals," *Jpn. J. Appl. Phys.* **42**, 3463-3466 (June, 2003).

Conference Proceedings:

1. H. Wang, X. Nie, T. X. Wu and S. T. Wu, "Cell gap effect on the dynamics of liquid crystal phase modulators," *11th Int. Meeting on Optics of Liq. Cryst.* p. 162, (Oct. 2005).
2. C. H. Wen, S. Gauza, J. Li, S. T. Wu, H. Wang, and X. Liang, "High-contrast homeotropic alignment of difluoro-tolane liquid crystals," *SID Digest* **36**, 1466-1469 (2005).
3. X. Nie, Y. H. Lin, H. Wang, Z. Ge, T. X. Wu, and S. T. Wu, "Polar anchoring energy measurement of vertically aligned liquid crystal cells," *SID Digest* **36**, 780-783 (2005).
4. T. X. Wu, Q. Hong, H. Wang, R. Lu, X. Zhu, Y. Huang, Z. Ge, and S. T. Wu, "Mathematical modeling of liquid crystal devices," *Int. Conf. Mathematical Methods in EM Theory* (IEEE Cat. No. 04EX840), pp. 82-87 (2004).
5. H. Wang, T. X. Wu, L. Zheng and S. T. Wu, "Efficient dynamic analysis of liquid crystal devices," *IEEE AP-S/URSI*, p. 109 (2004).
6. L. Zheng, T. X. Wu, H. Wang, W. Brokaw and S. T. Wu, "Smart liquid crystal microstrip shifter," *IEEE AP-S/URSI*, p. 20 (2004).
7. H. Wang, L. Zheng, J. Chen, T. X. Wu and S. T. Wu, "Smart millimeter-wave devices using liquid crystal," *Proc. SPIE* **5389**, pp. 476-485 (2004).
8. S. T. Wu, S. Gauza and H. Wang, "High birefringence liquid crystals for laser beam steering," *IEEE/LEOS* **2**, pp. 522-523 (2002).